chemosensors

MDPI

Review

Room-Temperature Surface Acoustic Wave Gas Sensors: Sensing Mechanisms, Functional Materials, and Performance Benchmarking

Cristian Viespe

Laser Department, National Institute for Laser, Plasma and Radiation Physics, Atomistilor 409, 077125 Magurele, Romania; cristian.viespe@inflpr.ro

Abstract

Room-temperature surface acoustic wave (SAW) gas sensors respond through several transduction mechanisms, but published analytical figures of merit are rarely directly comparable. This critical, non-systematic review examines mass, acoustoelectric, elastic and viscoelastic loading across hydrogen, methane, ammonia, nitrogen oxides, hydrogen sulfide, carbon oxides and selected vapors. The review draws on 32 selected study records and compares 16 configurations in detail, retaining native readout units, calibration definitions, minimum tested concentrations, author-reported limits of detection (LODs), humidity and optical activation. Studies were selected to illustrate the diversity of materials, acoustic architectures and analytical reporting practices rather than to provide exhaustive literature coverage. The analysis identifies inconsistent LOD arithmetic, conflicting sensitivity statements and substantial gaps between estimated thresholds and experimentally tested concentrations. Humidity-dependent polarity changes and aging further limit simple performance rankings. Calculated LODs, measured concentration boundaries and experimentally determined sensitivities are treated as distinct quantities. Further development requires direct low-concentration validation, reproducible noise statistics, mechanism-resolved measurements, matrix testing and system-level energy accounting.

Keywords: surface acoustic wave; room-temperature gas sensing; acoustoelectric loading; elastic loading; hydrogen; methane; ammonia; limit of detection; benchmarking; sensor metrology

1. Introduction

Reliable gas detection under ambient conditions is needed in industrial safety, environmental monitoring, hydrogen technologies, process analytics and distributed sensing networks. Hydrogen (H_2), methane (CH_4), ammonia (NH_3), hydrogen sulfide (H_2S), carbon monoxide (CO), carbon dioxide (CO_2), nitrogen oxides (NO and NO_2) and selected volatile organic compounds (VOCs) differ substantially in chemical reactivity, adsorption behavior, typical exposure scenarios and target concentration ranges. A sensitivity or detection-limit value alone is therefore insufficient for sensor selection. Selection also depends on matrix composition, humidity, drift, reversibility and the electrical architecture used to record an analyte-dependent signal.

Surface acoustic wave (SAW) devices detect physical changes within an acoustically accessible region of a piezoelectric structure. A gas-sensitive layer on the propagation path couples sorption and chemical processes to wave velocity, phase, attenuation or the oscillation frequency of an associated electronic circuit. This allows changes in material properties to be measured even when they do not produce a readily measurable direct electrical output. Unlike a standalone chemiresistor, a SAW device can respond to mechanical and electrical

Check for updates

Received: 12 October 2026
Revised: 9 November 2026
Accepted: 11 November 2026
Published: 13 November 2026

Copyright: © 2026 by the author. Licensee MDPI, Basel, Switzerland. This article is an open access article distributed under the terms and conditions of the Creative Commons Attribution (CC BY) license.

changes simultaneously, although this advantage also complicates attribution of the signal. Established reviews discuss mass, conductivity and elastic loading, the importance of nanostructured functional films and the range of gas-sensitive materials [1,2].

Compared with a chemiresistor, which requires an electrically measurable conducting path, a SAW transducer can interrogate sorption-induced mechanical changes in insulating or weakly conducting recognition films. Frequency and phase readouts also permit differential referencing, and suitable acoustic structures can be interrogated wirelessly. These capabilities broaden coating and packaging choices; they do not guarantee a lower detection limit, better selectivity or lower total power than a chemiresistor. SAW devices require control of temperature, film-induced attenuation and RF electronics, while chemiresistors can offer a simpler readout. A useful comparison therefore matches the target gas, humidity, calibration range, response time and complete energy budget [1,2].

Operation at room temperature may avoid continuous high-temperature heating of the active film and simplify the design of compact sensors. For this review, the nominal interval of 15–35 °C provides an operational definition, rather than a universal convention. The operating temperature alone, however, does not establish system-level power consumption: SAW oscillators require electrical energy; wireless devices require external radio-frequency interrogation; and optical activation may be necessary even when the film itself is not heated. UV-assisted results must therefore be distinguished from unilluminated devices and from performance reported only under thermal activation.

Materials investigated include Pd-based films and bilayers for H_2, carbon nanowalls and molecular host layers for CH_4, metal oxides and conducting polymers for NH_3, chalcogenide and graphene-derived layers for NO_2, copper-containing or zinc-containing reactive coatings for H_2S, and porous or molecularly selective structures for other gases and vapors. Previous reviews cover NO_2 nanomaterials, physical SAW sensing mechanisms, low-dimensional films and 2D-material SAW devices at room temperature [1–4]. Grouping results by material does not, however, establish whether the reported analytical figures of merit were obtained using comparable procedures.

Two recurring problems complicate comparison. First, sensitivity is published as Hz/ppm, kHz/vol%, mV/vol%, degree/ppm and related quantities; the reported coefficient may represent a fitted calibration slope, a secant through two points or a single response-to-concentration ratio. Second, a stated limit of detection (LOD) may be statistically extrapolated far below the smallest analyte concentration tested in the laboratory. Some reports specify baseline noise as a maximum excursion rather than a standard deviation, whereas others calculate a limit from a single signal-to-noise measurement. The resulting numbers cannot be ranked simply by their magnitude without knowing the calibration conditions and noise definition.

This review compares published SAW gas-sensing results by examining the acoustic readout and the evidence supporting each analytical claim. It preserves calibration intervals and native units, distinguishes author-reported LODs from minimum tested concentrations, and records humidity, activation and stability. The emphasis is on reproducibility and application-oriented validation rather than a numerical ranking of material families. The analysis considers whether sensitivity is a fitted slope or a point ratio, whether an LOD can be reconstructed from a defined noise statistic, whether the claimed threshold was experimentally tested, and whether proposed mechanisms have independent support. Table 1 compares this focus with that of selected prior reviews [1–4]. The distinctions concern primary focus and do not imply that earlier reviews omit analytical considerations.

The material strategies used today have an established history. Wohltjen and Dessy introduced SAW probes for chemical analysis in 1979 [5]. Wohltjen subsequently examined polymer-coated SAW vapor sensors, relating coating perturbations to acoustic response

and device design [6]. Ricco, Martin and Zipperian demonstrated conductivity-mediated sensing using a lead-phthalocyanine film on $LiNbO_3$, showing why a chemically responsive coating need not act solely as an added mass [7]. These foundational contributions motivate the present distinction between sorption-driven mechanical loading and acoustoelectric coupling. They provide historical context rather than additional room-temperature performance records in the 32-study comparison.

Table 1. Positioning of the present analysis against selected prior reviews; primary emphases are not mutually exclusive.

Review	Principal Emphasis	Scope/Comparative Emphasis
Dinu et al. (2022) [1]	Nanomaterials for NO_2 SAW sensors	Material/deposition strategies for one analyte
Li et al. (2023) [2]	SAW mechanisms and micro/nanostructured films	Mechanistic and materials overview
Lin et al. (2024) [3]	Low-dimensional SAW sensing materials	Functional-material classes and sensing applications
Reddeppa et al. (2025) [4]	2D-material room-temperature SAW sensors	2D materials and associated device performance
This review (2026)	Multi-gas critical evidence assessment	Noise/LOD traceability; tested minimum; readout and activation stratification

The alternating row shading is used only to improve readability.

2. Scope and Literature Selection

2.1. Scope and Operating Conditions

The review considers original investigations reporting a measured gas- or vapor-dependent SAW response at approximately 15–35 °C. Included acoustic architectures may use a delay line, resonator, oscillator, Love-wave waveguide, or a SAW device coupled to a phase-to-voltage or other readout circuit. A claim of high frequency or piezoelectric operation by itself does not establish a SAW measurement. Pure quartz-crystal microbalance (QCM), bulk acoustic wave and standalone chemiresistive outputs are not interchangeable with a SAW result; mixed-platform articles contribute only their clearly identified SAW data. Fabrication or annealing temperatures do not define operating temperature, and thermal regeneration temperatures are recorded separately from gas exposure temperatures.

The review covers H_2, CH_4, NH_3, H_2S, NO/NO_2, CO/CO_2, and selected VOCs; additional acid gases, oxygen and chemical-warfare simulant vapors are included for mechanistic or methodological contrast where RT SAW measurements are documented. A reported RT value is considered for discussion if accompanied by primary-source evidence of gas exposure; an explicit RT statement without a numeric temperature is retained with lower confidence. UV, visible-light and sunlight-assisted measurements are identified as separate experimental conditions and are not pooled with dark-operation data by default.

2.2. Literature Identification and Selection Criteria

This critical, non-systematic review focuses on literature published in 2015–2026, with a cutoff of 9 October 2026. Literature identification combined terms for surface acoustic waves and SAW sensors with gas detection, gas sensing, vapor sensing and the target analytes, supplemented by targeted searches and reference checking. Studies were selected purposively for a measured SAW gas response under room-temperature conditions, representation of different material and acoustic-device classes, and relevance to the interpretation of sensitivity, detection limits and operating conditions. Examples include carbon-nanowall SAW detection of H_2 and CH_4 [8], metal-functionalized TiO_2-based CH_4 sensing [9], and triethanolamine-based H_2S sensing [10].

Earlier foundational publications are cited selectively to explain the development of chemical recognition coatings and transduction mechanisms; they are outside the 2015–2026 performance-comparison dataset.

The detailed comparison includes 32 selected study records, of which 16 configurations are highlighted in the main-text tables. The selection emphasizes mechanistic and metrological contrasts rather than publication counts or exhaustive coverage. Background reviews and additional original studies support the broader discussion. Reports with incomplete operating-condition or analytical-method information are qualified explicitly; missing information is not interpreted as a negative sensing result. The selection does not define a systematic-review eligibility endpoint and is not used to calculate pooled performance estimates or population-level rankings.

2.3. Data Extraction and Quality Controls

For each representative configuration, the information sought included gas, sensing layer, substrate, acoustic mode, nominal frequency, operating temperature, carrier gas, relative humidity (RH), light or thermal activation, analyte range, minimum tested concentration, raw signal type, calibration sensitivity and its definition, author-reported LOD, noise statistic and method, response/recovery times, repeatability, selectivity and long-term stability. Data extraction gives priority to numerical methods, tables and figures over statements in the conclusions. Verification using accessible full-text passages is distinguished from corroboration based only on abstracts. Where different articles by the same group describe similar Pd/Ni nanowire architectures, independence of the underlying devices or datasets requires verification and is not assumed from distinct DOIs [11].

Sensitivities are retained in their original units because frequency, phase and electronically converted voltage readouts cannot be converted directly. Each reported sensitivity is identified as fitted slope, secant, response/concentration ratio or unspecified. The standard small-signal diagnostic form C_LOD = kσ_y/|b| is dimensionally valid only when σ_y represents blank-output fluctuations in the same signal units as the response and b is a local calibration slope in signal per concentration; it is not a substitute for a validated decision threshold, calibrated blank correction or uncertainty assessment. The coefficient k and noise statistic must be defined by the source. A standard error of the fitted slope has units of signal per concentration and cannot be substituted for σ_y in this expression. Four LOD labels are used in this review: LOD-S (an author-reported statistical estimator using a stated noise statistic and calibration slope); LOD-R (extrapolated from a stated signal-to-noise ratio at a test point); MTC (minimum tested concentration without an independently identified statistical LOD); and LOD-U (author-reported LOD with unresolved method or numerical discrepancy). These are review-specific descriptors, not adopted metrological standards. All source-reported values are retained even when an independent diagnostic substitution differs. Inclusion in Tables 3 and 4 is a presentation choice rather than an independent certification of source completeness. An author-reported LOD is considered independently validated only if the precise noise statistic, number of baseline samples, low-concentration calibration function and exposure conditions are reproducible from the accessible primary source. A maximum baseline deviation is not interchangeable with the standard deviation σ. Entries that cannot meet these requirements remain qualified as LOD-U or reported-only and are not used for numerical rankings. The label LOD-S identifies the reported calculation method, not independent validation of its statistical assumptions. The LOD-R label likewise denotes a source-derived single-point signal-to-noise extrapolation and is not a measured concentration boundary. For gas concentrations, 1 vol% = 10,000 ppm and 1 ppm = 1000 ppb when the quantities refer to the same gas-fraction basis; these conversions do not make different acoustic readouts commensurate.

AI tools assisted with preparing and checking comparison tables from the selected studies, checking calculations and citation numbering, and revising the methodological discussion and the reporting checklist in Table 5. Figure 3 was plotted from the numerical inputs in Table A4. The Acknowledgments identify the tools and model versions.

2.4. Basis and Limitations of the Comparison

Appendix A (Tables A1–A3) presents the 32 selected, DOI-linked study records underlying the detailed comparison. The 16 configurations in Tables 3 and 4 illustrate differences in acoustic readout, target gas, proposed mechanism, illumination, humidity and analytical reporting. These examples show how experimental conditions affect comparisons; they do not identify a sensing material that is superior under all conditions. Author-stated room temperature and numerical operating temperatures are distinguished, and incomplete source information is reported explicitly.

2.5. Publication Overlap and Evidence Independence

Each distinct DOI is counted once as a bibliographic record, but a DOI does not necessarily represent an independent device, measurement set or proof of repeatability. The 2015 Cu^{2+}/PANI/WO_3 NO paper reports testing in dry nitrogen, whereas the related 2017 paper explicitly cites those earlier nitrogen results and reports a newly optimized film tested in dry air. Thus, the previously published nitrogen dataset is not counted again as independent replication. For the Pd/Ni nanowire architecture [11], device and dataset provenance should be established before nominally similar reports are treated as independent replication. Such independence is not certified in this review. For devices measured using both SAW and chemiresistive or other non-SAW methods, only acoustic-channel results are eligible for the SAW comparisons. The purposive selection and source-specific information gaps limit the scope of inference; distinct publications are not treated automatically as independent experimental replication.

3. SAW Fundamentals and Device Architectures

3.1. Acoustic Transduction and Signal Variables

A propagating surface wave in a piezoelectric medium has a mechanical displacement field that decays away from the surface and, where piezoelectric coupling is significant, an accompanying electric field. A functional coating therefore perturbs both mechanical and electrical boundary conditions. To the first order, a small relative change in propagation velocity may be written $\Delta v/v_0$, while the accumulated propagation phase $\theta = 2\pi fL/v_0$ has the first-order change $\Delta\theta \approx -(2\pi fL/v_0)(\Delta v/v_0)$ at fixed frequency f and acoustic path length L. With the usual transmission convention $\arg(S_{21}) = -\theta$, the corresponding transmission-phase change has the opposite sign. In an oscillator operated near a stable mode, $\Delta f/f_0$ frequently tracks changes in effective acoustic velocity, but the proportionality depends on resonator loading, insertion phase, loop electronics and the definition of the tracked oscillation point. An oscillator shift must not be interpreted automatically as a direct intrinsic SAW-velocity change.

For a coating that is thin compared with the acoustic wavelength and has modest coupling, mass-loading perturbation models often predict a frequency decrease upon added surface mass. However, electrical loading, film elasticity, waveguide redistribution and thermal effects can alter both the magnitude and sign of the measured signal. In particular, a reported positive acoustic frequency shift during gas exposure cannot be dismissed as anomalous without checking elastic and acoustoelectric pathways. General derivations and the limitations of simplified models are reviewed elsewhere [2]; the discussion here concerns the parameters needed for a reliable comparison of experimental performance.

3.2. Delay Lines, Resonators and Oscillator Circuits

A two-port delay line places a sensing film between input and output interdigital transducers (IDTs). It can support phase, group-delay and transmission-amplitude readouts and provides access to insertion loss as well as phase. Interpretation depends on the electrical port conditions, the frequency at which the phase is evaluated, and whether the baseline incorporates differential reference-channel compensation. Resonators use reflected acoustic energy or periodic structures to define resonance; frequency shifts are often easier to track but may be affected by resonance quality factor, frequency locking strategy and film-induced damping. Oscillator systems close an electrical loop around an acoustic component, converting acoustic phase/velocity changes into a frequency count. This readout enables Hz-scale reporting but may introduce drift and electronic frequency pulling that should be controlled using matched reference devices.

Figure 1 traces the measurement from controlled gas exposure through a coated SAW delay line and its electronic readout to calibration and concentration estimation. The response must be calibrated against known concentrations under matched temperature, RH and activation conditions; an acoustic shift alone is not a concentration measurement.

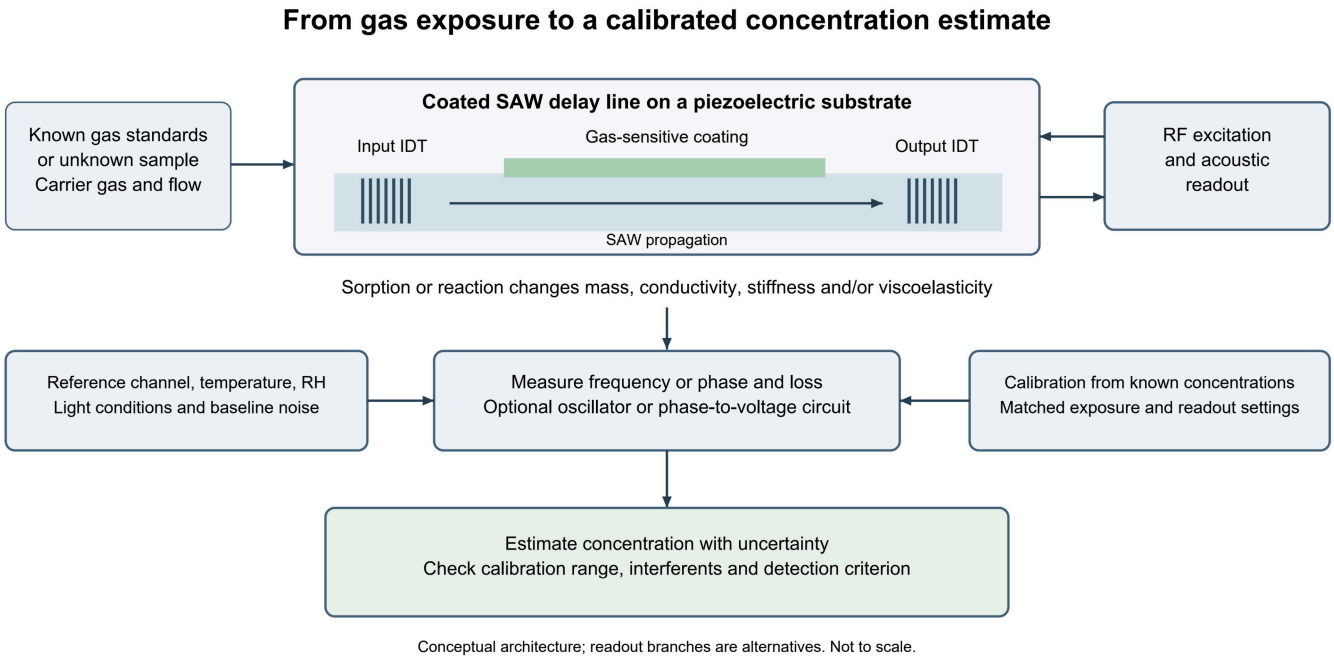


Figure 1. Conceptual measurement chain for SAW gas sensing and concentration estimation. Gas interactions alter coating properties and thereby the acoustic observables. Reference and environmental measurements support compensation, while known gas standards establish the calibration. The delay-line, oscillator and phase-to-voltage readouts are alternative implementations; no numerical device performance is implied. The diagram was drawn in Python 3.12 with ReportLab using code generated in OpenAI Codex (GPT-6.1 Sol).

Phase discriminators and phase-to-voltage circuits require separate consideration. For example, the Pd/Ni nanowire H_2 device reports 1.65 mV/vol% at room temperature [11], whereas a Pd/ZnO oscillator-based result is expressed in Hz/ppm [12]. These sensitivities are not directly comparable even after a simple concentration-unit conversion unless the transduction gain, linearity, baseline-noise bandwidth and circuit stability are established. Conversely, the SnO_2/CuO CO_2 device measures voltage after phase conversion; its sensitivity must be treated as the system-level response rather than an intrinsic surface mass sensitivity [13].

3.3. Wave Modes, Substrates and Frequency

ST-cut quartz is attractive for frequency and temperature stability, whereas $LiNbO_3$ and related piezoelectric platforms can provide relatively strong coupling but require careful thermal and electrical control. Langasite and AlN-based structures offer additional substrate and operating-frequency choices. Love-wave devices use a guiding layer to confine shear-horizontal energy near the surface, making them advantageous for certain soft, polymeric or liquid-adjacent sensing configurations. They should nevertheless be benchmarked as guided-wave devices with specific waveguide and attenuation properties rather than grouped indiscriminately with Rayleigh-wave oscillators. The Ag/PPy Love-wave VOC study illustrates the diversity of modes and response units [14].

At a fixed fractional velocity change, frequency shifts tend to scale with carrier frequency, although film thickness relative to wavelength, mode confinement, insertion losses and electronics can change the actual relationship. Consequently, devices at 100 MHz, 200 MHz, 860 MHz or several GHz cannot be ranked by raw Hz/ppm alone. Normalized $\Delta f/f_0$ or phase-per-length information can aid mechanistic comparison, but only when the corresponding response definition and calibration conditions are provided. A rigorous benchmark therefore records the frequency and mode alongside the published sensor signal.

3.4. Differential Architectures and Reproducibility

Differential delay lines or dual resonators can compensate common-mode effects such as ambient temperature and oscillator drift, provided that sensing and reference structures have comparable acoustic and electrical characteristics. A reference film that also sorbs water or the target gas may instead create a composite signal with reduced interpretability. Reports should specify the reference coating, oscillator loop topology, electrical bandwidth and logging rate. Critical performance metrics include baseline noise at the measurement timescale, chip-to-chip distribution, drift, recovery and the selectivity test protocol, in addition to the maximum measured frequency shift. Table 2 summarizes these architectures and their principal readout qualifications.

Table 2. Comparison of common SAW architectures; examples are descriptive, not device-specific performance claims.

Architecture	Primary Observable	Strength	Main Qualification
Two-port delay line	Phase/insertion loss/ group delay	Can inspect multiple propagation observables	Electrical terminations, path length and interrogation frequency matter
Resonator	Resonance frequency/Q	Compact narrowband tracking	Film loading and resonance damping must be separated
Oscillator with SAW element	Closed-loop oscillation frequency	Straightforward Hz counting and reference channels	Loop gain/phase, oscillator pulling, electronics noise
Love-mode waveguide	Shear-wave phase and/or frequency	Energy confinement near sensing film	Guiding-layer geometry and viscoelastic losses
Phase-to-voltage/ wireless	Electrical output after SAW conversion	System integration and RF readout	mV/ppm depends on transfer function and gain

The alternating row shading is used only to improve readability.

4. Gas-Sensing Mechanisms

4.1. Mass Loading and Adsorption Kinetics

Gas adsorption or reaction can increase surface mass, generally slowing the acoustic wave when other boundary conditions remain unchanged. Thin-film perturbation models are useful, but their interpretation is less straightforward for strongly porous films, nanowire networks or coatings with appreciable mechanical and electronic changes. Sorption capacity,

film thickness and porosity regulate both signal amplitude and access of gas molecules to active regions, while adsorption/desorption kinetics and gas-cell mixing influence response time. Strong analyte binding may favor a signal magnitude yet reduce reversibility. The frequent practice of equating any negative frequency shift with "mass loading" should therefore be considered a tentative interpretation unless the individual contributions have been separated experimentally.

4.2. Acoustoelectric Loading and Heterogeneous Junctions

The piezoelectric field accompanying a SAW interacts with mobile charge in a conductive overlayer. Adsorbate-induced charge transfer, redox reactions and carrier mobility changes can therefore alter acoustic velocity and attenuation. The sign and magnitude depend on conductivity relative to the acoustoelectric coupling regime and on the substrate/device configuration; a universal mapping from gas type to frequency-shift polarity does not exist. Pd/ZnO for H_2 was explicitly discussed in terms of combined mass and interfacial acoustoelectric effects, and more recent heterogeneous SnO_2/CuO CO_2 systems similarly emphasize interfacial electronic modulation [12,13]. Independent sheet-resistance measurements under identical gas/RH conditions provide a stronger basis for this attribution than a SAW trace alone.

4.3. Elastic and Viscoelastic Loading

A chemical reaction or sorption event can stiffen or soften the functional film. Since the acoustic displacement penetrates the coating, a change in effective modulus, density or interfacial shear coupling can reverse the sign expected from added mass. The ZnO/Al_2O_3 H_2S study attributes a positive-frequency response to elastic loading associated with surface chemistry; the assignment is physically plausible but requires comparison with independent evidence for stiffness change and reaction products [15]. Likewise, PbS quantum-dot functionalization for NO_2 changes both the sign and kinetics of the acoustic response, consistent with an important change in coating properties but insufficient in itself to isolate a single mechanism [16].

Polymeric films introduce viscoelastic behavior that can couple frequency, phase and insertion loss. Penetrant-induced plasticization, swelling, changes in relaxation time and film thickness can all affect a Love-wave response. The polymer and GO-based SAW vapor studies reveal useful chemical affinities, but their reported sensitivity is conditional on specific operating RH and waveguide properties [14,17]. When electrical conductivity is negligible, the absence of acoustoelectric loading does not imply that only inert mass adsorption matters; viscoelastic dispersion can still dominate.

4.4. Evidence Hierarchy and Interpretation

This review distinguishes (i) independent mechanistic support, such as a reproducible electrical-resistance trace and surface analysis under appropriate controls; (ii) evidence indirectly consistent with a mechanism, such as concentration-dependent acoustic polarity plus a post-exposure chemical signature; and (iii) a mechanism proposed chiefly from an assumed adsorption pathway or signal sign. An experimental demonstration that a coating is chemiresistive does not prove that its SAW response is acoustoelectrically dominated unless the acoustic and electrical data are coherently related. A comparison of CuO/Al_2O_3 H_2S sensing with both acoustic and chemiresistive readouts is useful in this context, but the measured metrics from the two transducers must not be merged into a single SAW performance entry [18]. Published attributions of a mass, elastic, viscoelastic or acoustoelectric contribution are labeled as mechanistic interpretations unless a separate

and relevant experimental observable discriminates those competing mechanisms; phase or frequency sign alone does not meet this standard.

Relative humidity reverses the frequency response of the room-temperature CuO/AlN NH_3 sensor. The authors discuss competing acoustic and electrical contributions, indicating that humidity modifies the sensing mechanism rather than simply adding a constant offset [19]. These observations justify measuring SAW response, electrical properties and surface chemistry under matched conditions, preferably with a reference channel and multiple RH values. Figure 2 summarizes the four mechanism families and emphasizes their possible coexistence.

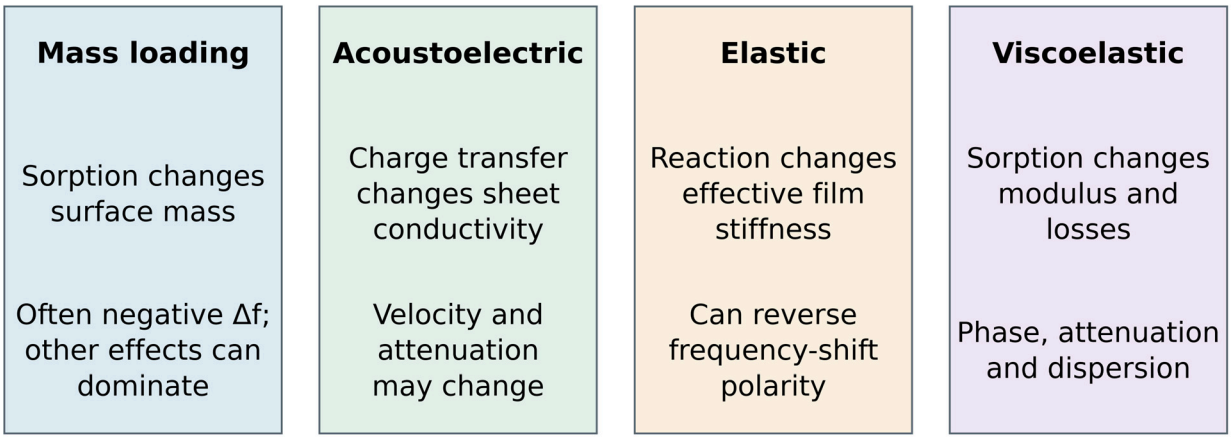


Figure 2. Conceptual pathways for SAW gas transduction. This original schematic summarizes the mechanisms discussed in Section 4. Several pathways may coexist; response sign alone does not establish the dominant mechanism.

5. Functional Materials and Gas-Specific Applications

5.1. Hydrogen: Catalytic Metal/Semiconductor and Nanowire Architectures

Hydrogen sensors are dominated by Pd-containing coatings because hydrogen uptake and dissociation modify Pd-based surface chemistry and electronic properties. A Pd/ZnO bilayer fabricated using pulsed laser deposition (PLD) was reported with 0.51 Hz/ppm sensitivity and a published 59 ppm LOD, while measurements covered 0.2–2 vol% H_2 [12]. This is an extrapolated threshold; the lowest measured hydrogen concentration was 2000 ppm. Pd/SnO_2 films were subsequently reported with 0.21 Hz/ppm and a 142 ppm estimated LOD over a similar 0.2–2 vol% test interval [20]. For Pd/TiO_2 porous layers, the original study reports approximately 0.10 Hz/ppm and a 1210 ppm LOD, illustrating that a high surface area does not automatically imply superior quantitative performance across different acoustic configurations [21].

Nanowire and alloy devices illustrate different trade-offs. A Pd–Ni alloy-film SAW sensor was tested at 25 °C down to 0.01 vol% (100 ppm) H_2; its reported sensitivity of 21.3 kHz/vol% and estimated LOD below 10 ppm must be interpreted with the actual noise statistic and test window in view [22]. A Pd/Ni nanowire system using a phase discriminator reports response times of approximately two seconds in a relatively high 0.3–3.5 vol% interval, but its voltage sensitivity is not directly comparable to frequency-based devices [11]. Pd/Cu nanowires were likewise investigated for rapid room-temperature H_2 sensing, with attention to alloy composition and conducting pathways [23]. Related publications from the same group require checks for dataset independence before they are treated as indepen-

dent demonstrations. Polymer/quantum-dot coatings offer a complementary H_2 strategy, although their acoustic transduction and calibration must be evaluated separately [24].

5.2. Methane: Carbon Nanostructures, Molecular Hosts and Oxide Composites

Selective methane sensing at low temperature is difficult because of its weak polarity and modest room-temperature interaction with many conventional oxides. A cryptophane A-functionalized room-temperature SAW resonator uses a molecular recognition approach, with approximately 204 Hz/vol% sensitivity but measurements starting at 0.2 vol% and an estimated detection limit of approximately 0.05 vol% (about 500 ppm) [25]. The chemistry is selective in concept, but its use for trace detection in the field requires reproducible calibration in atmospheres containing realistic interferents.

Carbon nanowalls treated by plasma were reported for both H_2 and CH_4 on a SAW platform. For CH_4, the published 18 Hz/ppm value at 200 ppm and estimated 4.17 ppm LOD were obtained with a minimum tested CH_4 concentration of 200 ppm; the numerical gap must remain visible in any performance table [8]. A separate Pd-functionalized W,V-doped TiO_2/polyethyleneimine composite was characterized over 0.4–2 vol% CH_4, with 1.79 Hz/ppm and an estimated 17 ppm LOD; a 4000 ppm lower test bound precludes claiming direct validation at 17 ppm [9]. More recently, a monolayer GO SAW methane study reported measurements extending to 1 ppm, but sensitivity values given for the low-concentration interval differ between the main discussion (0.19 mV/ppm) and conclusions (0.06 mV/ppm); the abstract separately reports 0.046 mV/ppm for 100–1000 ppm. The differences must not be silently resolved as one global slope without the original calibration fit and electronic gain [26].

5.3. Ammonia: Polymers, Oxides and Hybrids

NH_3 studies show why a high initial response alone does not establish reliable analytical performance. The rGO/DPP2T-TT SAW sensor reports 55 Hz/ppm sensitivity over 500–1400 ppb, with a 425 ppb estimated LOD obtained from a particular signal-to-noise calculation; approximately 54% of the original response remained after 31 days in the reported aging test [27]. A polyacrylic acid (PAA) resonator exhibits different reported calibration slopes, about 750 Hz/ppm in 0.5–2 ppm and 400 Hz/ppm in 2–20 ppm, demonstrating that concentration interval is intrinsic to the sensitivity value [28].

For metal-oxide SAW sensors, the room-temperature NH_3 response of a TiO_2 coating depends strongly on humidity: the response near 10 ppm at 80% RH should not be combined uncritically with the concentration–calibration data recorded at 50% RH [29]. ZnO nanorods have also been compared with unstructured ZnO films, illustrating enhancement of the signal at the cost of relatively slow recovery at some NH_3 levels [30]. In MoS_2-based devices, a reported 4878 Hz/ppm coefficient corresponds closely to the response/concentration ratio at 5 ppm, while the response varies nonlinearly across 5–50 ppm [31]. The MoS_2 paper also states that its detection limit could be below 1 ppm, without a reproducible statistical derivation in the inspected passage; this claim is retained as LOD-U rather than treated as demonstrated sub-ppm detection [31].

Hybrid AuNPs–Cu_2O/rGO/PPy films have been reported with 2 Hz/ppb sensitivity and 8 ppb calculated LOD; the minimum tested point of 12 ppb is comparatively close to the estimate but the reported 8 ppb threshold follows a 12 ppb single-point signal-to-noise extrapolation (352 Hz response, 75 Hz stated noise), rather than the global reported 2 Hz/ppb coefficient. A direct $3 \times 75/(2$ Hz/ppb) substitution gives 112.5 ppb, demonstrating that these two published quantities are not interchangeable for a statistical LOD; the definition of the 75 Hz noise is not sufficient to certify either threshold independently [32]. A CuO-decorated AlN SAW resonator achieved a reported 24 ppb NH_3 LOD at around 26 °C with

5/25 s response/recovery, while also showing RH-dependent polarity inversion [19]. Material screening should therefore consider how RH and aging affect the response, alongside the lowest reported dry-air detection limit. An AuNP-decorated graphene/polypyrrole NH_3 sensor also shows the need to examine calibration scatter and extrapolated LOD values rather than relying only on the reported ppb limit [33].

5.4. Nitrogen Oxides and Hydrogen Sulfide

For NO_2, g-C_3N_4 nanosheet coatings on langasite were reported to exhibit roughly −3.1 kHz at 100 ppm and an estimated 158 ppb LOD near 27 °C [34]. UV-activated g-C_3N_4 nanoribbons produce much larger signals at tested ppm concentrations and a reported approximately 42 ppb LOD, but these photoassisted measurements belong to a distinct energy/activation class; the article title uses the term "sub-ppb", whereas its numerical abstract gives an estimated LOD of about 42 ppb; the numerical value is retained [35]. PbS quantum-dot surface treatment changed a NO_2 response from a negative to a positive frequency shift at the same 10 ppm challenge, demonstrating material-induced changes to acoustic transduction beyond a simple mass-only description [16].

Graphene derivatives may use a phase readout: a bilayer-graphene NO_2 device reported 0.29°/ppm and an estimated 68 ppb LOD, whereas sulfur-doped graphene was reported at 0.19°/ppm with an estimated 140 ppb LOD; these are not directly comparable to frequency sensitivities [36]. A Pt nanocluster/GO device reports a minimum experimentally tested concentration of 20 ppb, compared with an independently reported 6.6 ppb estimated LOD and 45.4 mV/ppm sensitivity [37]. For NO, the Cu^{2+}/PANI/WO_3 publications report distinct environmental test matrices: the earlier study demonstrates ppb-level sensing in dry N_2 [38], while the later paper evaluates a modified composition in dry air [39] and recapitulates the earlier nitrogen findings. The dry-nitrogen observations must not be counted twice as independent sensing experiments. For bilayer graphene, the results report 0.29°/ppm but the conclusion gives 0.2°/ppm; the published definition of σ as the standard error of the regression slope in $3.3\sigma/S$ is dimensionally problematic: both σ and the calibration slope S have units of degrees per ppm, so their ratio is dimensionless, not a concentration. The quoted 68 ppb and 140 ppb author LODs therefore remain unverified pending identification of an output-noise or response-residual statistic with appropriate units [36].

H_2S-responsive films often rely on metal-sulfide formation or changes in oxide-film mechanics and electronic properties. A ZnO/Al_2O_3 composite exhibited a positive response at 10 ppb H_2S, interpreted as enhanced elastic loading [15]. CuO/Al_2O_3 has been analyzed using both SAW and chemiresistive configurations, demonstrating that separate transduction pathways must be identified before comparing performance [18]. A sol–gel CuO coating showed a stronger H_2S response under high humidity, contrary to the assumption that water always suppresses the analytical signal [40]. Room-temperature H_2S sensing with triethanolamine films supplies an additional complementary chemical strategy [10]. Porous SnO_2/SiO_2 acoustic coatings offer an additional H_2S material architecture, with performance that should be interpreted through its own mass and humidity conditions [41].

An optically activated Bi_2S_3 device illustrates the need for textual consistency checks: the article gives approximately 95.2 ppb in its three-sigma calculation but 31.8 ppb in the conclusion. Using the baseline standard deviation of 0.0344 kHz and the slope of 1.08306 kHz/ppm fitted to $|\Delta f|$ over 0.5–8 ppm, $3\sigma/S \approx 0.0953$ ppm (95.3 ppb), while $\sigma/S \approx 0.0318$ ppm (31.8 ppb). Thus the values reflect a factor-of-three discrepancy, not independently demonstrated detection thresholds; the 500 ppb minimum experimental challenge remains separate [42].

5.5. CO, CO_2, VOCs and Specialized Vapors

Room-temperature CO measurements with a Pd–Pt/SnO_2/Al_2O_3 film have been reported at 25 °C and 50% RH over 10–100 ppm. Acoustic shifts of approximately 1.1 kHz at 10 ppm and 13.6 kHz at 100 ppm should not be reduced to a global linear calibration without inspecting intervening points and the noise model [43]. A SnO_2/CuO heterojunction SAW phase-to-voltage device for CO_2 tested 0.1–4 vol% at 25 °C, reporting a sensitivity of 11.35 mV/vol% with 9.3/28.9 s response/recovery; its signal cannot be treated as a frequency slope [13]. The Au/TiO_2/PEDOT platform measured CO_2 and RH at 20 °C with a contribution from sunlight-assisted operation, requiring separate identification of optical conditions [44].

For VOCs and chemical simulants, molecular affinity and waveguide design can be as important as the adsorption capacity of nanomaterials. Ag-modified polypyrrole Love-wave sensors reported separate acetone, ethanol and toluene response characteristics; for acetone, a nominal 3 ppb estimated LOD should be read alongside a 500 ppb experimental lower bound and strong RH suppression [14]. GO Love-wave sensors for DMMP and DPGME report different LODs and sensitivity coefficients for each analyte within one paper, supporting per-gas rather than per-publication performance entries [17]. Hydroxyl-rich sol–gel $AlO_x(OH)_\gamma$ SAW layers demonstrate a strong HCl response at 25 °C, with water-assisted uptake and film processing conditions playing central roles [45]. Specialized analytes broaden mechanistic understanding but should not distort conclusions about common industrial monitoring targets. Oxygen-responsive Zn–Fe oxide coatings broaden the family of RT SAW sensing demonstrations, but should not be conflated with reducing-gas selectivity claims [46].

5.6. Selecting a Functional Coating for the Target Application

No material class is most suitable for every SAW gas sensor. For H_2, Pd-containing films and metal/oxide hybrids provide catalytic dissociation and hydrogen uptake, but selection must also consider hysteresis, oxidation and recovery [11,12,20–23]. For weakly interacting CH_4, molecular hosts such as cryptophane A offer recognition sites, whereas carbon and oxide composites require careful validation of selectivity and low-concentration calibration [8,9,25,26]. Polymers and acid-functional layers can provide affinity for NH_3 and vapors, but water sorption, swelling and aging may alter both calibration and acoustic loss [14,27,28]. Oxides, low-dimensional semiconductors and their hybrids offer electrical or reactive pathways for NH_3, NO_2 and H_2S; humidity-dependent polarity and potentially incomplete chemical reversibility must be tested for the intended exposure matrix [15,18,19,34,40].

The preferred coating is therefore the one that combines appropriate analyte affinity with reversible kinetics, stable adhesion and acceptable acoustic attenuation on the chosen substrate and wave mode. Thickness relative to wavelength, accessible porosity, sheet conductivity and viscoelasticity must be optimized together. Increasing surface area or electrical conductivity is not intrinsically beneficial: excessive film loading can dampen the wave, and conductivity changes must occur within a useful acoustoelectric coupling regime. Material selection should use matched-condition measurements of sensitivity, uncertainty, interferents, RH response, recovery and retained calibration after aging, rather than the lowest reported LOD alone [1,2].

6. Humidity, Stability and Selectivity

6.1. Relative Humidity as a Coupled Variable

Water affects several processes that contribute to the SAW response. It competes for adsorption sites, changes surface protonation and the conductivity of hydrophilic layers, changes capillary uptake in porous networks, and modifies viscoelastic or elastic properties.

The net acoustic signal may therefore be suppressed, enhanced or reversed depending on the operating RH. A CuO/AlN ammonia device shows polarity inversion with RH, while sol–gel CuO and TiO_2 films reveal humidity-enhanced responses for H_2S or NH_3 under certain conditions [19,29,40].

Cross-study comparisons should state both RH and carrier gas at each response point. Measurements in dry N_2, synthetic air, laboratory air and controlled humidified air are chemically different systems. Oxygen and water can modify surface charge states, Pd oxidation, adsorption equilibrium and product desorption. A reported 4200 Hz NH_3 shift at 80% RH is not an interchangeable calibration point in a series measured at 50% RH. At minimum, studies intended for deployment should report a two-dimensional response surface in concentration and RH, together with a reference or compensation strategy and appropriate uncertainty estimates.

6.2. Response/Recovery Time and Exposure Dynamics

Response and recovery durations are often reported without a common threshold convention. T90 is the time to 90% of a defined step amplitude, while t10–t90 rise times and visually estimated plateau times measure different phenomena. Gas-cell residence time, line dead volume, flow rate, chamber mixing, diffusion within the film and electronic filtering all affect the measured response. A response of a few seconds in an optimized high-concentration H_2 experiment cannot be assumed to persist at trace levels or in humid mixtures. Similarly, slow recovery for strongly interacting polymer or nanostructured coatings may require thermal, optical or purge-assisted regeneration that changes system-level energy consumption.

6.3. Aging, Baseline Drift and Device-to-Device Variation

Long-term suitability cannot be inferred from repeated exposure cycles over a single session. The rGO/DPP2T-TT NH_3 device exhibited considerable response attenuation over one month; by contrast, a Pd–Ni H_2 alloy study reported more favorable longer-term variation under its own test protocol [22,27]. These are not directly comparable durability metrics because gas challenge, RH, storage conditions, measurement frequency and aging procedure differ. Reports should include the number of devices and cycles, time since coating deposition, baseline drift rate, periodic zero-gas recalibration, RH, target concentration, and uncertainty for retained sensitivity. Mechanistic monitoring of Pd oxidation is also relevant to aging and regeneration of hydrogen sensing layers, even when regeneration is performed at a temperature above the sensing interval.

Stability within the proposed 15–35 °C operating interval requires separate assessment of reversible temperature dependence and irreversible aging. Even without a film heater, temperature changes affect acoustic velocity, oscillator drift, adsorption equilibrium and coating modulus; optical activation can also raise the local film temperature. A suitable validation protocol would record the actual sensing-region temperature, measure blank and gas-exposed responses at several controlled temperatures across the interval, and repeat calibration after temperature/RH cycles and storage. Matched reference channels should be evaluated for residual compensation error. Response retention at one temperature does not establish stability throughout 15–35 °C, and this review does not certify that interval for every listed device. The available aging examples [22,27] support material-specific conclusions under their reported conditions.

6.4. Selectivity and Multi-Gas Conditions

Selectivity measured against one interferent at a single arbitrary concentration is weaker evidence than a matrix study reproducing expected field mixtures. Responses

should ideally be compared using relative challenge concentrations appropriate to the application, not only equal ppm amounts. Adsorption competition and humidity-mediated chemistry can produce nonlinear mixture effects. An array architecture or multivariate classifier can improve gas discrimination, but it does not replace the need to characterize each underlying SAW element and validate performance under independent mixtures. Comparisons should distinguish intrinsic selective binding, differential/reference readout, and algorithmic discrimination as three distinct contributions.

7. Performance Benchmarking and Critical Comparison

7.1. Why Simple Sensitivity Rankings Fail

Published SAW sensitivity is not a universal device-independent quantity. A frequency oscillator, fixed-frequency phase discriminator, resonator peak tracker and voltage-converted delay line measure related but nonidentical response variables. Even within one readout type, a quoted sensitivity may represent a fitted slope, a secant between two endpoints, or the ratio between one response and its gas concentration. The distinction can be seen in the MoS_2 NH_3 results: a 24,389 Hz response at 5 ppm gives 4877.8 Hz/ppm as a one-point ratio, whereas a secant between the published 5 and 50 ppm response data is approximately 1851 Hz/ppm. These values reflect different definitions and calibration spans; neither can be assigned indiscriminately to the full operating range [31].

The issue is not limited to high-sensitivity devices. Graphene-oxide CH_4 studies have reported different voltage sensitivity coefficients for high and low concentration ranges, with an unresolved difference between a low-concentration value in the results discussion and its corresponding conclusion [26]. The comparison therefore records native units and the precise concentration range, while assigning a distinct status to estimated, measured and ambiguous figures of merit.

7.2. LOD, Signal-to-Noise Ratio and Demonstrated Detection

A common formal LOD estimate is LOD = $3\sigma/|S|$, where σ is a well-defined baseline standard deviation measured under relevant conditions and S is the local fitted calibration slope. For a non-linear calibration, the effective slope must correspond to the low-concentration region over which extrapolation is intended. A maximum deviation from a trend line or a peak-to-peak noise width is not statistically identical to σ; multiplying such a quantity by three may be unjustified. In some articles, the LOD is instead inferred from a single concentration and a signal-to-noise ratio, namely C_test × (target SNR)/(observed SNR). These estimators may differ even when the authors' calculations are internally coherent.

For the Pd/ZnO H_2 sensor [12], the reported sensitivity was 0.51 Hz/ppm and the estimated LOD was 59 ppm. The lowest tested concentration was 2000 ppm. These values illustrate the distinction between a calculated threshold and the experimentally tested range. An earlier Pd/WO_3 example [47] also illustrates the importance of specifying the noise definition.

A more explicit within-paper discrepancy occurs for the Bi_2S_3 H_2S sensor under yellow-light activation: the methods specify SD = 0.0344 kHz from 300 baseline points and fitted S = 1.08306 kHz/ppm for |Δf| over 0.5–8 ppm. The stated 3SD/S expression gives approximately 0.0953 ppm (95.3 ppb), consistent with the reported 95.2 ppb in the calculation section, whereas the conclusion cites 31.8 ppb, approximately one-third of that result [42]. Without a published clarification, Table 4 shows both as a disputed report (LOD-U) and does not pick the more favorable value. Conversely, for Pd/SnO_2 the stated approximate 10 Hz noise and 0.21 Hz/ppm sensitivity reproduce an LOD near 143 ppm [20], while the lowest hydrogen exposure remains about 2000 ppm. Numerical consistency of an extrapolation should not be confused with validation at the estimated concentration. The source does

not establish that its approximate noise value is a baseline standard deviation, so numerical consistency alone does not justify classifying this Pd/SnO_2 result as an independently validated statistical LOD.

7.3. Experimental Validation Gap

The ratio G = C_min,measured/LOD_reported describes the separation between the lowest experimentally tested concentration and the author's calculated limit, provided both concentrations are expressed in compatible units. G does not independently establish whether an LOD is correct. It is sensitive to the choice of tested concentrations, the author's LOD definition and whether the response is linear near the inferred threshold. In CH_4 examples, plasma-treated carbon nanowalls report a 200 ppm minimum test versus a 4.17 ppm calculated LOD (G ≈ 48), while W,V:TiO_2/Pd–PEI reports 4000 ppm versus 17 ppm (G ≈ 235) [8,9]. By comparison, the NH_3 AuNPs–Cu_2O/rGO/PPy report gives 12 ppb minimum test versus 8 ppb LOD (G = 1.5) [32].

A high G indicates a lack of direct validation near the reported LOD; it does not establish an error in the calculation. A report of 20 ppb experimentally demonstrated versus 6.6 ppb estimated for Pt nanocluster/GO NO_2 sensing illustrates comparatively transparent reporting [37]. Reporting both values helps readers assess whether detection at low concentrations has been tested and reproduced. Figure 3 illustrates the concentration-to-LOD gap for ten study records from Tables A1–A3, with both conflicting H_2S limits shown separately.

A further example is the 2026 monolayer GO/CH_4 report [26]. An approximately 1 ppm methane concentration was tested in the low-range experiment, so that concentration is a measured lower bound of the reported series, not proof that the statistical LOD was independently determined to be 1 ppm. The article reports a low-range sensitivity of approximately 0.19 mV/ppm in its results discussion but 0.06 mV/ppm in the conclusions; the results and conclusion associate these values with 1–20 ppm and should not be silently reconciled. The high-range fitted value, approximately 0.046 mV/ppm for 100–1000 ppm, is a different calibration domain.

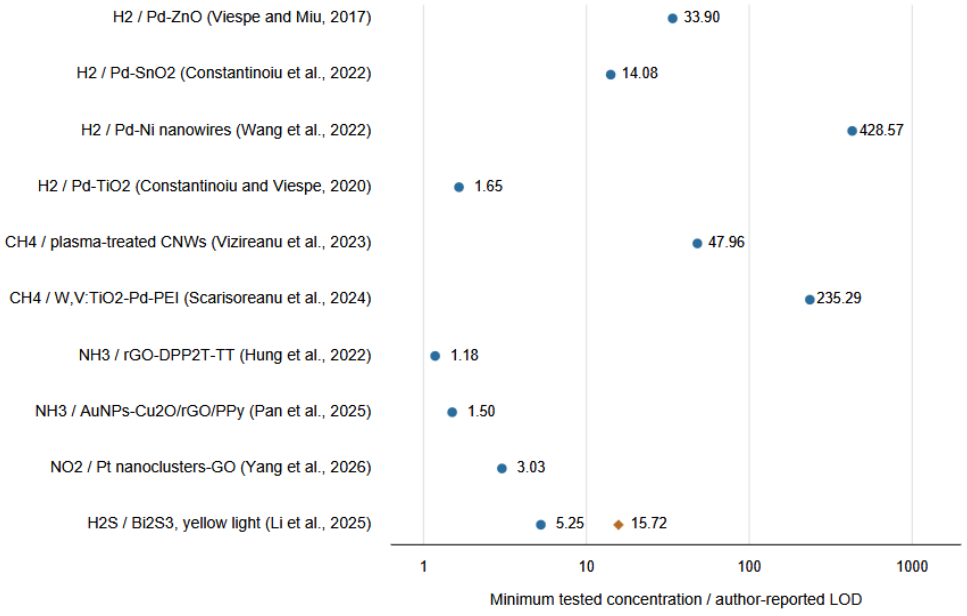


Figure 3. Illustrative ratio G of minimum tested concentration to author-reported LOD for ten study records in Tables A1–A3 [8,9,11,12,20,21,27,32,37,42]. Concentrations in each ratio share the same gas-fraction units. For Bi_2S_3, the circle uses the calculation-section value of 95.2 ppb and the diamond

the conflicting conclusion value of 31.8 ppb. Both remain disputed author reports. Ratios are descriptive validation gaps, not cross-gas performance rankings; the source values and reproducible ratios are given in Table A4. The plot was redrawn from Table A4 using Python and ReportLab code produced with OpenAI Codex (GPT-6.1 Sol) during revision to update the reference labels. The plotting inputs were the concentrations and detection limits tabulated for the cited studies.

7.4. Comparison Across Gases and Experimental Conditions

Tables 3 and 4 summarize the operating conditions and analytical evidence for 16 purposively selected SAW configurations; the detailed 32-study comparison is provided in Appendix A (Tables A1–A3). Both frequency- and voltage-based readouts, different sample gases and optically assisted experiments are reported in their original terms so that differences between experiments remain explicit. No ranking across gases or acoustic modes is attempted. The comparison identifies three recurring limitations: (i) CH_4 detection limits extrapolated well below the lowest tested concentrations, (ii) NH_3 responses that change with RH, nonlinear calibration or aging, and (iii) claimed ppb-level performance whose noise criterion is not always independently reproducible. CO_2 performance at percent concentrations is not interpreted as equivalent to ppb-level environmental NO_2 monitoring.

Table 3. Representative room-temperature SAW sensing architectures ($n = 16$) and context-dependent outputs. RT denotes the author-stated room temperature where no numeric value was extracted; "n.v." means not verified in the examined source. Values labeled as single-point response must not be interpreted as global calibration slopes.

Gas [Ref.]	Sensing Architecture/ Film	Temperature/ Activation	Carrier/ Humidity	Readout	Published Sensitivity or Response
H_2 [12]	Pd/ZnO; quartz SAW oscillator, ~69.5 MHz	RT stated; lighting n.v.	synthetic air; RH n.v.	frequency/Δf	0.51 Hz/ppm (mean Δf/c)
H_2 [22]	Pd–Ni 40 nm; 160-MHz $LiNbO_3$ delay line, differential loop	25 °C; optical input not reported	N_2; RH n.v.	oscillation frequency	21.3 kHz/vol% (fit)
CH_4 (also H_2) [8]	Plasma-treated carbon nanowalls; quartz SAW oscillator, ~62 MHz	RT stated; illumination n.v.	RH and carrier not verified	frequency	18 Hz/ppm at 200 ppm
CH_4 [9]	W,V:TiO_2/Pd–PEI; quartz SAW oscillator, ~69 MHz	RT stated; illumination n.v.	RH and carrier not verified	frequency	1.79 Hz/ppm (author)
NH_3 [27]	rGO/DPP2T-TT; ST-X quartz SAW resonator, 98.5 MHz	24 °C; no light reported	dry air	frequency	55 Hz/ppm
NH_3 [28]	PAA/200-MHz SAW oscillator	20 °C; no light reported	30% RH reference	frequency	750 vs. 400 Hz/ppm; different ranges
NH_3 [32]	AuNPs–Cu_2O/rGO/PPy; ST-cut quartz SAW resonator, 98.5 MHz	RT stated; optical status n.v.	dry air; RH also studied	frequency	2 Hz/ppb (fitted, claimed)
NH_3 [31]	MoS_2; 128° Y-cut $LiNbO_3$ SAW delay line, 122 MHz	RT stated; lighting n.v.	RH n.v.	frequency	4878 Hz/ppm (5 ppm ratio)
NH_3 [19]	CuO NPs/AlN SAW resonator	26 °C; lighting n.v.	RH 5–80%; sign reversal	frequency	+52.6 kHz at 100 ppm (point)
NO_2 [35]	g-C_3N_4 nanoribbons/SAW	~30 °C; UV (365 nm)	RH 0–80% studied	frequency	~28.13 kHz at 10 ppm
NO_2 [37]	Pt nanoclusters/GO SAW	RT stated; lighting n.v.	RH n.v.	phase-to-voltage	45.4 mV/ppm (author)
H_2S [15]	ZnO/Al_2O_3/SAW	RT stated; lighting n.v.	RH n.v.	frequency	~+500 Hz at 10 ppb
H_2S [42]	Bi_2S_3/SAW	24 ± 1 °C; 590 nm light, 20 μW/cm^2	60% RH	frequency	1.08306 kHz/ppm (|Δf| fit, 0.5–8 ppm)
CO [43]	Pd–Pt/SnO_2/Al_2O_3/SAW	25 °C; 12-V circuitry	50% RH	frequency	1.1 kHz at 10 ppm; 13.6 kHz at 100 ppm
CO_2 [13]	SnO_2/CuO/$LiNbO_3$ SAW delay line	25 °C; light not stated	dry synthetic air; RH varied separately	phase-to-voltage	11.35 mV/vol% (author)
VOC [14]	Ag/PPy Love wave	24 °C; light n.v.	dry air; 30% RH depresses response	frequency	910 Hz/ppm (acetone)

n.v. = not verified in the examined source. The alternating row shading is used only to improve readability.

Table 4. Analytical evidence for the same 16 configurations, in the order of Table 3. Published LOD values remain author claims, not independently certified detection thresholds. LOD-U flags unresolved methods or numerical inconsistencies; MTC is the minimum tested concentration, not an independently validated statistical LOD.

Gas [Ref.]	Tested Range	Minimum Measured	Author-Reported LOD	Evidence Class	Qualification/Limitation
H_2 [12]	0.2–2 vol% H_2	0.2 vol% = 2000 ppm	59 ppm	Reported estimate	Published LOD estimate: 59 ppm. Minimum tested: 2000 ppm
H_2 [22]	0.01–0.04 vol%	0.01 vol% (100 ppm)	<10 ppm in results; 10 ppm conclusion	LOD-U	<10 ppm results vs. 10 ppm conclusion; 100 ppm min test
CH_4 (also H_2) [8]	200–1000 ppm CH_4	200 ppm CH_4	4.17 ppm (CH_4, reported)	LOD-U	3n/S, $n \approx 25$ Hz; statistic unresolved; 200 ppm minimum challenge
CH_4 [9]	0.4–2 vol% CH_4	0.4 vol% = 4000 ppm	17 ppm	LOD-U	3n/S, $n \approx 10$ Hz; statistic unresolved; 4000 ppm minimum challenge
NH_3 [27]	500–1400 ppb NH_3	500 ppb	425 ppb [est.]	LOD-R	SNR-derived LOD; ~46% response loss by day 31
NH_3 [28]	0.5–50 ppm NH_3	0.5 ppm (500 ppb)	0.5 ppm (published limit)	MTC	500 ppb is the lowest challenge, not a statistical LOD
NH_3 [32]	12–1000 ppb NH_3	12 ppb	8 ppb	LOD-R	At 12 ppb: signal 352 Hz, stated noise 75 Hz, SNR = 4.69 ⇒ C_LOD ≈ 7.7 ppb; global 2 Hz/ppb gives a different diagnostic
NH_3 [31]	5–50 ppm NH_3	5 ppm	<1 ppm (qualitative author claim)	LOD-U	No reproducible LOD derivation; 5 ppm minimum tested; 4878 Hz/ppm is a point ratio
NH_3 [19]	100 ppm response point	n.v.	24 ppb	LOD-U	Measured shift at 100 ppm ≠ global sensitivity
NO_2 [35]	10 ppm response point	n.v.	42 ppb	LOD-U	UV-assisted; title says sub-ppb, abstract LOD 42 ppb
NO_2 [37]	n.v.	20 ppb NO_2	6.6 ppb (reported $3\sigma/k$)	LOD-S (author)	20 ppb measured; 6.6 ppb statistically estimated
H_2S [15]	n.v.	10 ppb (response shown)	n.v.	No LOD extracted	Positive shift; independent elastic proof incomplete
H_2S [42]	0.5–50 ppm H_2S	0.5 ppm = 500 ppb	95.2 ppb (methods); 31.8 ppb (conclusion)	LOD-U	$3 \times 0.0344/1.08306 \approx 95.3$ ppb; $0.0344/1.08306 \approx 31.8$ ppb; 500 ppb experimentally challenged
CO [43]	10–100 ppm	10 ppm	n.v.	No LOD extracted	Endpoint slope diagnostic; 12 V is the electronics supply
CO_2 [13]	0.1–4 vol% CO_2	0.1 vol%	n.v.	MTC (not LOD)	CO_2 only; 0.1 vol% lowest challenge
VOC [14]	0.5–5 ppm acetone; ethanol/toluene also tested	0.5 ppm = 500 ppb acetone	3 ppb acetone (est.)	LOD-U	SNR ≥ 3 criterion reported; noise statistic/calculation incomplete; 500 ppb minimum test

n.v. = not verified in the examined source. The alternating row shading is used only to improve readability. The arrow (⇒) indicates the change from the untreated to the treated sensing layer. Both frequency shifts were measured at 10 ppm NO_2.

7.5. Toward Comparable Reporting

Comparable reporting requires the following information: substrate/mode and f_0; the complete electronic transfer function; temperatures of sensing, fabrication and regeneration separately; carrier gas, RH and illumination; at least three independently fabricated chips where possible; calibration points with replicate variance and detection-model fit; raw baseline-noise recording duration and statistic; both estimated LOD and minimum tested concentration; separately defined T90 response/recovery; and multiweek drift or recalibration behavior. These recommendations concern the measurements needed to compare numerical results across laboratory designs; they do not require every proof-of-concept device to meet field-certification criteria.

Table 5 translates these recommendations into a reporting template for future SAW gas-sensor manuscripts. Authors should state when an item was not measured or is not applicable, and distinguish repeated cycles on one device from independently fabricated chips.

Table 5. Suggested reporting checklist for room-temperature SAW gas sensors. The items support transparent comparison and do not constitute a certification standard.

Reporting Item	Information to Report
Acoustic device and coating	Substrate/cut, mode, f_0, IDT geometry, coating composition, thickness, deposition and reference channel.
Readout and acquisition	Frequency, phase, loss or voltage; transfer function/gain; bandwidth, filtering, logging rate and oscillator topology.
Exposure conditions	Measured sensing temperature, carrier gas, gas-fraction basis, RH, pressure, flow and cell volume; fabrication and regeneration temperatures separately.
Optical or thermal activation	Wavelength, irradiance at the film, illuminated area, electrical input, duty cycle and local temperature; dark/control measurements.
Calibration and sensitivity	Concentration points and range, independent exposure replicates, fitted model and residuals, uncertainty; slope versus point ratio and native units.
Noise and detection evidence	Raw blank duration, sample count, bandwidth and noise statistic; LOD equation, coefficient and inputs; minimum tested concentration and near-threshold validation.
Dynamics and reversibility	Response/recovery definition, gas delivery and purge timing, concentration/RH, incomplete recovery and any reset procedure.
Selectivity and environmental response	Interferent concentrations, realistic mixtures, RH/temperature dependence and residual error after compensation.
Repeatability and stability	Independent chip/batch counts, repeated cycles, sensor age, storage, retained calibration, baseline drift and recalibration frequency.
System energy and data models	Energy per valid reading including light/readout/reset/reader; for learned models, grouped/time-separated splits, training-only preprocessing and independent test errors.

The alternating row shading is used only to improve readability.

8. Challenges, Research Gaps and Future Perspectives

8.1. Separating the Contributions to the SAW Response

The major mechanistic challenge is separating mass, acoustoelectric, elastic and viscoelastic contributions in the same experiment. To separate these contributions, experiments could combine measurement of the SAW signal with simultaneous electrical sheet-conductivity monitoring, controlled adsorption mass measurements where feasible, and independent chemical or mechanical characterization. Measurements over controlled humidity ranges, oxygen concentration variation and reference layers would clarify whether signal polarity changes originate from surface transport, film modulus or electronic operating-point shifts. Because film morphology affects the acoustic energy distribution, theoretical models should report wave mode, boundary conditions and thickness-to-wavelength ratio rather than invoke a universal mass-loading law.

8.2. Low-Concentration Validation and Metrological Transparency

In several reports, a low LOD is extrapolated from calibration at concentrations tens or hundreds of times higher. Further measurements should test concentrations in the vicinity of the declared threshold and report both blank false-positive rates and detection probability under a defined decision rule. Use of replicate chips, confidence/prediction intervals and appropriate calibration models will make LOD estimates more meaningful than simplified three-sigma arithmetic alone. Where nonlinear behavior is observed, authors should report local sensitivities by range rather than one peak- or low-concentration ratio as a universal device parameter.

8.3. Operating Conditions and Energy Accounting

Temperature-independent gas adsorption cannot be assumed; neither can a claim of heater-free sensing be interpreted as zero power. Active SAW oscillators, microcontrollers, wireless links, UV LEDs and regulated supplies each contribute to the duty-cycle energy budget. For wireless/passive interrogated devices, external reader energy and link reliability are operational variables even when the sensing tag contains no battery. Future reports should quantify energy per reading, warm-up/reset time, illumination power and wavelength, and the extent to which a selective signal is maintained when light or heating is removed. These factors are especially relevant to distributed leak monitoring, occupational safety wearables and remote installations.

A useful reporting boundary is the energy required for one valid concentration result over a defined measurement cycle of duration τ: $E = \int P(t)\,dt\ (0 \le t \le \tau)$, where $P(t)$ is the sum of RF/readout, illumination, control, communication and auxiliary power. The average power is E/τ. The cycle should include warm-up, acquisition, purge/reset and standby, and identify whether gas-delivery auxiliaries and the external wireless interrogator are included. When one cycle yields several valid readings, the number of readings and the allocation of shared energy must be stated. Optical irradiance at the film multiplied by illuminated area gives incident optical power; it is not the LED electrical input, which also depends on the source and driver efficiency and coupling losses. LED supply voltage/current, illumination time and duty cycle should therefore accompany wavelength and irradiance. Continuous RF excitation, amplification, frequency counting or phase conversion can set a persistent readout power demand, while switching the circuit off may introduce restart and settling costs. Consequently, removal of the film heater is an architectural advantage, but a total-energy advantage over a heated sensor requires measurements under matched sampling intervals and performance requirements.

8.4. Reproducible Materials and Scalable Packaging

Reproducibility between laboratories depends on control of coating thickness, porosity, doping and metal oxidation state; PLD or hydrothermal growth conditions; IDT geometry and passivation; and packaging-induced stress or contamination. Development beyond a proof of concept requires quantification of device-to-device variation and assessment of batch repeatability, environmental aging, vibration, temperature cycling and interference from common industrial mixtures. Differential channels and integrated electronics may improve robustness, but only if their reference response and compensation error are independently evaluated. A stable sensor module with integrated electronics represents a different stage of development from a functioning SAW chip.

8.5. Data-Driven Calibration and Its Limitations

Machine learning can use multichannel SAW amplitude, phase, frequency and environmental measurements for compensation or recognition of gas patterns. Performance should be assessed using independent devices and measurements at sensor ages, gas mixtures and humidity conditions excluded from training. Overfitting to a small number of laboratory exposures can falsely improve apparent selectivity. Interpretability is particularly important when acoustic mechanisms evolve with RH or aging; models should identify out-of-distribution operating regimes and propagate uncertainty rather than provide concentration estimates with unjustified confidence.

For SAW exposure series, validation splits should follow the intended use and the dependence structure of the data. All samples and overlapping windows from one exposure cycle should remain in the same fold. Leave-one-device-out or leave-one-batch-out validation can assess transfer to a new chip or fabrication batch, while forward-in-time

testing, with an appropriate gap between training and test blocks, can assess aging and recalibration. Complete RH/temperature conditions or gas-mixture compositions may be withheld to test generalization beyond the calibration matrix; this is a distinct and more demanding task than interpolation. Hyperparameter tuning and feature selection should use an inner grouped validation loop within each outer training set. Scaling, baseline correction learned from data and dimensionality reduction must likewise be fitted only on training data. An untouched final test set should contain independent devices or later exposure sessions where available. Authors should report the number of independent devices and exposures per split, per-condition concentration bias and error, uncertainty coverage, and false-positive/detection rates near the decision threshold. Randomly splitting neighboring time points from the same gas pulse is liable to leak correlated information and overstate performance. These are proposed validation protocols; they are not results of a model fitted in this review.

8.6. Specific Research Priorities

The reviewed studies indicate four priorities: (i) agreed definitions and sufficient raw information for sensitivity and LOD; (ii) mechanism-oriented simultaneous acoustic, electrical and environmental measurements; (iii) lifetime and matrix validation near application-relevant concentrations; and (iv) integrated module benchmarks that include electronics, power, calibration maintenance and communications. Assessment of a large frequency shift must also establish whether the response is traceable, selective, reversible and reproducible beyond a single optimized test condition.

9. Conclusions

Room-temperature SAW gas sensors convert molecular adsorption and reaction processes into acoustic responses through mass, electrical, elastic and viscoelastic loading. A wide range of metal oxides, catalytic metals, carbon derivatives, polymers, low-dimensional materials and hybrid films have demonstrated measurable responses to H_2, CH_4, NH_3, NO_x, H_2S, CO/CO_2 and selected vapors. These results establish scientific feasibility for several important analytes, but they do not support a universal ranking based on the smallest author-reported LOD or largest raw sensitivity coefficient.

Three limitations recur in the comparison. First, published responses use non-equivalent readouts and calibration definitions, and a ratio between one measured shift and its concentration cannot automatically replace the fitted response slope over a wide interval. Second, many LODs are extrapolated below the lowest experimentally investigated concentrations, sometimes using incompletely documented noise statistics; numerical discrepancies and conflicting statements within individual publications must be identified explicitly rather than corrected without explanation. Third, relative humidity, optical activation, carrier gas, film aging and acoustic architecture can modify both the magnitude and physical origin of a reported response. Sensor performance must therefore be interpreted as a property of the material–SAW–electronics–environment system.

Sixteen representative configurations are compared in complementary main-text tables, with a detailed 32-study comparison in Appendix A (Tables A1–A3). The purposive selection illustrates differences in sensing mechanisms, readouts, operating conditions and analytical evidence. The conclusions apply to these documented examples and methodological issues; they do not constitute an exhaustive literature assessment or a pooled ranking of room-temperature SAW sensors.

Progress toward practical use requires clear definition of wave mode and readout, direct testing at low concentrations, traceable baseline-noise statistics, calibrated humidity/light conditions, independent mechanistic support and replicated long-term testing. Combining

physical interpretation with metrological evidence would allow room-temperature SAW sensors to be compared by their reproducibility and practical performance. The comparisons illustrate differences in reporting quality; they neither assess all laboratories nor provide a statistically pooled performance estimate. Table A5 records the diagnostic calculations and the limitations that cannot be resolved from the published data.

Funding: This work was supported by the Romanian Ministry of Education and Research through the project "Excellence Center of Advanced Responsive Materials" (PN-IV-P6-6.1-CoEx-2024-0187, contract no. 12CoEx/2026) and by the National Authority for Research and Innovation through the Nucleus Programme LAPLAS VII (grant no. 30N/2023) and PoCIDIF (no. 390008/27.11.2024).

Institutional Review Board Statement: Not applicable.

Informed Consent Statement: Not applicable.

Data Availability Statement: No new experimental gas-sensing data were generated for this review. The extracted study-level values, analytical qualifications and numerical inputs underlying the comparison figure are included in the manuscript, particularly Tables A1–A5. DOI links to the original studies are provided in the reference list. Raw experimental time series from the cited publications were not available for independent reanalysis.

Acknowledgments: The author used OpenAI ChatGPT (GPT-6) and Codex (GPT-6.1 Sol and GPT-6 Astra) to help correct the wording of the manuscript, prepare and check table entries against the cited studies, and verify calculations and citation numbering. During revision, these tools also assisted with the additional methodological passages, the historical references added to the introduction, the reporting checklist in Table 5, and the Python code for Figures 1 and 3. The author reviewed and edited the AI-assisted material, made the final decisions about the scientific content and its interpretation, and takes full responsibility for the manuscript.

Conflicts of Interest: The author declares no conflict of interest.

Appendix A. Detailed Study-Level Evidence

Tables A1–A3 document the same 32 selected study records and retain their native units, calibration domains, minimum tested concentrations and analytical qualifications. The records are presented in a consistent order across the three tables. Reference numbers identify the original publications and their DOI links in the reference list. "n.v." means not verified in the examined source. An author-stated room temperature without a numerical value is not converted into an assumed temperature. No LOD listed here is independently certified from raw experimental data. Table A5 documents the main arithmetic inconsistencies within sources, unit checks and cases of non-independent data using the reference numbers in this manuscript.

Evidence terminology follows Section 2: LOD-S denotes an author-reported statistical estimate with an identified noise/slope expression; LOD-R denotes a reported signal-to-noise estimate; LOD-U denotes an unresolved method or discrepancy; and MTC denotes a minimum tested concentration rather than a statistical LOD. These codes classify reporting evidence. A fitted slope, an average $\Delta f/c$ and a single-point response/concentration ratio remain different sensitivity definitions.

Table A1. Sensing architectures and operating conditions for the 32 selected study records. Optical assistance is stated separately from sensing temperature.

Gas [Ref.]/Sensing Layer	Acoustic Device/ Substrate	Sensing Temperature/ Optical Status	Humidity/Gas Matrix
H_2 [12] Pd/ZnO bilayer PLD	Quartz SAW oscillator; ~69.5 MHz	Room temperature stated; numerical temperature not reported Optical: No optical activation stated in checked passages	Synthetic air; RH not verified
H_2 [20] Pd/SnO_2	Quartz SAW oscillator; approximately 69 MHz	Room temperature stated; numerical temperature not reported Optical: n.v.	Synthetic air; 0.5 L/min total flow; RH not reported in the examined methods
H_2 [22] Pd–Ni alloy, 40 nm	SAW delay line + differential oscillator	25 °C Optical: No optical activation reported	Pure N_2 carrier
H_2 [11] Pd/Ni nanowires	200 MHz SAW delay-line + phase discriminator	25 °C Optical: n.v.	Humidity dependency studied
H_2 [21] PLD porous Pd/TiO_2 bilayer; Pd-1500/TiO_2-600	Quartz SAW, f0 n.v.	Room temperature explicit Optical: Fabrication by PLD; no illumination during sensing stated	n.v.
CH_4 (also H_2) [8] Carbon nanowalls/ plasma-treated	Quartz SAW oscillator; ~62 MHz	Room temperature stated by publisher Optical: n.v.	n.v.
CH_4 [9] W,V:TiO_2/Pd–PEI (S9)	Quartz SAW oscillator; ~69 MHz	Room temperature stated by publisher Optical: n.v.	n.v.
CH_4 [26] Monolayer graphene oxide (GO), ~1.1 nm	Y-cut quartz SAW delay line/voltage readout	Room temperature, numeric °C not confirmed Optical: No UV reported	N_2 purge; RH not reported in the examined methods
CH_4 [25] Cryptophane A (drop-coated)	ST-X quartz, 2-port resonator + differential oscillator	20 °C Optical: No external optical stimulation stated	N_2/CH_4; at 5% CH_4 0/20/30% RH: 1015/1258/1381 Hz
NH_3 [27] rGO/DPP2T-TT	ST-X quartz SAW resonator; 98.5 MHz; differential oscillator readout	24 °C Optical: No illumination reported; dry air	Dry air; additional RH characterization identified as future work
NH_3 [28] Polyacrylic acid (PAA)	200 MHz SAW resonator + oscillator	20 °C Optical: No illumination during sensing; dried film at 60 °C during preparation	30% RH reference; 30/56/84% RH investigated
NH_3 [32] AuNPs–Cu_2O/rGO/PPy	ST-cut quartz SAW resonator; 98.5 MHz; dual-track configuration	Room temperature stated; numerical temperature not reported Optical: n.v.	Dry air for calibration; RH dependence also investigated
NH_3 [31] Hydrothermal MoS_2 nanospheres/ nanoflowers	128° Y-cut $LiNbO_3$ SAW delay line; 122 MHz	Room temperature stated; numerical temperature not reported Optical: No illumination indicated in checked passage	n.v.
NH_3 [29] TiO_2 sol–gel thin film	ST-cut quartz; two-port SAW resonator, 199.325 MHz after coating; oscillator readout	Room temperature; numerical value not given in checked passages Optical: No optical assistance reported; annealing at 300 °C during fabrication	50% RH for 1–100 ppm calibration; separate 10/50/80% RH comparison at 10 ppm
NH_3 [30] ZnO nanorods vs. ZnO nanofilm control	ST-cut quartz oscillator, f0 ~199.76 MHz (NRs)	25 °C Optical: No UV during sensing	25% RH
NH_3 [19] CuO nanoparticle/AlN	SAW resonator	26 °C Optical: n.v.	5–10% RH positive frequency shift; 20–80% RH negative
NO_2 [34] g-C_3N_4/LGS	SAW, type not verified	27 °C Optical: n.v.	20–80% RH tested
NO_2 [35] g-C_3N_4 nanoribbons	SAW, type not verified	30 °C Optical: UV 365 nm	0–80% RH tested
NO_2 [16] PbS quantum dots (before/after $Pb(NO_3)_2$ treatment)	n.v.	Room temperature stated; numerical temperature not reported Optical: n.v.	n.v.

Table A1. *Cont.*

Gas [Ref.]/Sensing Layer	Acoustic Device/ Substrate	Sensing Temperature/ Optical Status	Humidity/Gas Matrix
NO_2 [36] Bilayer graphene/ sulfur-doped graphene	n.v.	24 °C Optical: n.v.	n.v.
NO_2 [37] Pt nanoclusters/GO	n.v.	Room temperature stated; numerical temperature not reported Optical: n.v.	n.v.
NO [39] Cu^{2+}/PANI/WO_3	n.v.	Room temperature stated; numerical temperature not reported Optical: n.v.	Dry-air carrier
NO [38] Cu^{2+}/PANI/WO_3	n.v.	Room temperature stated; numerical temperature not reported Optical: n.v.	Dry N_2 carrier
H_2S [15] ZnO/Al_2O_3	n.v.	Room temperature stated; numerical temperature not reported Optical: n.v.	n.v.
H_2S [42] $Cu(NO_3)_2$-treated Bi_2S_3 nanoribbons	n.v.	24 ± 1 °C Optical: 590 nm light, 20 μW/cm^2; dark operation measured separately	60% RH; static gas exposures in an 18 L chamber
H_2S [18] CuO/Al_2O_3	n.v.	Room temperature stated; numerical temperature not reported Optical: n.v.	n.v.
CO [43] Pd–Pt/SnO_2/Al_2O_3	High-frequency SAW, f0 n.v.	25 °C Optical: 12 V circuit; light not stated	50% RH; 25–75% RH interference
CO_2 [13] SnO_2/CuO bilayer	200 MHz SAW delay-line, phase-to-voltage circuit	25 °C Optical: n.v.	Dry synthetic air matrix; 450 mL/min; RH varied in separate tests
CO_2 [44] Au/TiO_2/PEDOT	204 MHz delay-line SAW	20 °C Optical: Sunlight-assisted	RH: 5–90% independently studied
VOC (acetone/ethanol/ toluene) [14] Ag nanoparticle modified PPy Love-wave guide	Love-wave SAW/SiO_2 waveguide	24 °C Optical: No UV	Dry, 10% and 30% RH; synthetic air
DMMP/DPGME [17] Graphene oxide	Love-wave SAW	Room temperature stated Optical: Not established	Synthetic air
HCl [45] Sol-gel AlOx(OH)y film, 198 nm	SAW; f0 n.v.	25 °C Optical: Annealed at 300 °C during fabrication; sensing at 25 °C	40% RH

n.v. = not verified in the examined source. The alternating row shading is used only to improve readability.

Table A2. Analytical figures of merit for the same 32 records in the order of Table A1. Published sensitivities and LODs are retained as source reports, with their definitions and evidence classes. Concentrations and native output units are retained without unreported conversions.

Gas [Ref.]	Readout/Reported Sensitivity/ Calibration Definition	Measured Interval	Minimum Tested	Author LOD/ Evidence Class
H_2 [12]	Oscillation-frequency shift 0.51 Hz/ppm (reported Δf/c, average across 0.2–2%) Definition: Average response/concentration, not necessarily regression slope	0.2–2 vol% H_2	0.2 vol% = 2000 ppm	59 ppm (reported estimate). Minimum tested: 2000 ppm.
H_2 [20]	Oscillation-frequency shift 0.21 Hz/ppm Definition: Average Δf/c over the tested concentrations, not a fitted global slope	0.2–2 vol% H_2	0.2 vol% = 2000 ppm	142 ppm LOD-U (approximate 10 Hz noise not established as σ)

Table A2. *Cont.*

Gas [Ref.]	Readout/Reported Sensitivity/ Calibration Definition	Measured Interval	Minimum Tested	Author LOD/ Evidence Class
H_2 [22]	~270 Hz at 0.01 vol% 21.3 kHz/vol% Definition: Fitted calibration slope	0.01–0.04 vol%	0.01 vol% (100 ppm)	<0.001 vol% predicted in results; 0.001 vol% in conclusion (not reconciled) LOD-U: baseline ±5 Hz not proven σ
H_2 [11]	n.v. 1.65 mV/vol% Definition: not established from the available source information	0.3–3.5 vol% H_2	0.3 vol% = 3000 ppm	7 ppm (reported) LOD-U (procedure unresolved)
H_2 [21]	~1.8 kHz at 2 vol% H_2 0.10 Hz/ppm (average $\Delta f/c$) Definition: Mean single-point $\Delta f/c$ ratios across exposures, not independent global fit	0.2–2 vol% H_2	0.2 vol% = 2000 ppm	1210 ppm LOD-U (3n/S plausible; noise statistic unclear)
CH_4 (also H_2) [8]	Oscillation-frequency shift 18 Hz/ppm at 200 ppm CH_4 (reported) Definition: Pointwise response/concentration ratios; 18 Hz/ppm at 200 ppm	200–1000 ppm CH_4	200 ppm CH_4	4.17 ppm (CH_4, reported) LOD-U (3n/S; n = 25 Hz, statistic not established)
CH_4 [9]	Oscillation-frequency shift 1.79 Hz/ppm (reported) Definition: Average response/concentration ratios across 0.4–2 vol%	0.4–2 vol% CH_4	0.4 vol% = 4000 ppm	17 ppm (reported) LOD-U (3n/S; n≈10 Hz, statistic not established)
CH_4 [26]	~0.9 mV at 1 ppm; 4.8 mV at 20 ppm 0.046 mV/ppm (100–1000 ppm); 0.19 mV/ppm (1–20 ppm, Figure 4 of ref [26]); conclusion 0.06 mV/ppm (1–20 ppm) Definition: Separate calibration slopes; major internal inconsistency at 1–20 ppm	1–20 ppm and 100–1000 ppm separately	1 ppm	1 ppm; response actually shown at 1 ppm LOD-U (procedure unresolved)
CH_4 [25]	~50 Hz at 0.2 vol%; ~1 kHz at 5 vol% ~204 Hz/vol% Definition: Linear fit 0.2–5 vol%, R^2~0.99827	0.2–5 vol% CH_4	0.2 vol% = 2000 ppm	≈0.05 vol% (≈500 ppm) author-estimated; source section statements differ LOD-U (procedure unresolved)
NH_3 [27]	Oscillation-frequency shift: +35 Hz at 500 ppb 55 Hz/ppm Definition: Calibration slope over 500–1400 ppb; R^2 ≈ 0.9238	500–1400 ppb NH_3	500 ppb	425 ppb (estimated) LOD-R (single-point SNR estimate)
NH_3 [28]	+225 Hz at 0.5 ppm 750 Hz/ppm (0.5–2 ppm); 400 Hz/ppm (2–20 ppm) Definition: Separate calibration slopes, different concentration intervals	0.5–50 ppm NH_3	0.5 ppm (500 ppb)	0.5 ppm (published limit) MTC (measured concentration, not statistical LOD)
NH_3 [32]	Oscillation-frequency shift: 352 Hz at 12 ppb 2 Hz/ppb Definition: Author-reported calibration sensitivity over 12–1000 ppb; LOD derived separately from the 12 ppb signal-to-noise ratio	12–1000 ppb NH_3	12 ppb	8 ppb LOD-R (single-point SNR estimate)
NH_3 [31]	24,389 Hz at 5 ppm; 107,668 Hz at 50 ppm 4878 Hz/ppm reported Definition: Matches single-point ratio 24,389/5; 5–50 ppm endpoint secant ~1851 Hz/ppm	5–50 ppm NH_3	5 ppm	<1 ppm (qualitative author claim; calculation not reproduced) LOD-U (claimed threshold; derivation unresolved)

Table A2. *Cont.*

Gas [Ref.]	Readout/Reported Sensitivity/ Calibration Definition	Measured Interval	Minimum Tested	Author LOD/ Evidence Class
NH_3 [29]	500 Hz at 1 ppm (RH 50%); 3200 Hz at 100 ppm (RH 50%); 4200 Hz at 10 ppm (RH 80%) n.v. Definition: Different RH protocols; no reliable global slope extracted	1–100 ppm NH_3	1 ppm (500 Hz at 50% RH)	1 ppm described as detection limit; statistical derivation unverified MTC (measured concentration, not statistical LOD)
NH_3 [30]	NR: −1094 Hz at 100 ppm; film −307 Hz at 100 ppm 11.3 Hz/ppm nanorods; 3.0 Hz/ppm nanofilm Definition: Fitted slope equations at 10–100 ppm	10–100 ppm	10 ppm	LOD not reported in relevant passage No statistical LOD identified in checked source passage
NH_3 [19]	+52.60 kHz at 100 ppm NH_3 n.v. Definition: not established from the available source information	100 ppm response point	n.v.	24 ppb (reported) LOD-U (procedure unresolved)
NO_2 [34]	−3.1 kHz at 100 ppm NO_2 n.v. Definition: not established from the available source information	100 ppm point	n.v.	158 ppb LOD-U (procedure unresolved)
NO_2 [35]	≈28.13 kHz at 10 ppm NO_2 n.v. Definition: not established from the available source information	10 ppm response point	n.v.	42 ppb LOD-U (procedure unresolved)
NO_2 [16]	−2.2 kHz untreated → +9.8 kHz treated at 10 ppm NO_2 n.v. Definition: not established from the available source information	n.v.	n.v.	n.v. NR/not independently established
NO_2 [36]	n.v. Bilayer graphene: 0.29°/ppm in results/abstract; 0.2°/ppm in conclusion. S-doped graphene: 0.19°/ppm. Definition: Fits over 0.5–2.4 ppm (bilayer) and 0.3–2 ppm (S-doped)	0.5–2.4 ppm (bilayer graphene); 0.3–2 ppm (S-doped graphene)	0.5 ppm (bilayer); 0.3 ppm (S-doped)	68 ppb; 140 ppb LOD-U (regression statistic definition unresolved)
NO_2 [37]	n.v. 45.4 mV/ppm Definition: not established from the available source information	n.v.	20 ppb NO_2	6.6 ppb (reported 3σ/k) LOD-S (author reports noise/slope criterion)
NO [39]	165 Hz at 1 ppb NO n.v. Definition: not established from the available source information	At least 1 ppb NO tested	1 ppb NO	n.v. NR/not independently established
NO [38]	Relative response $\Delta f/f_0 = 4.3$ ppm at 1 ppb NO n.v. Definition: not established from the available source information	At least 1 ppb NO tested	1 ppb NO	n.v. NR/not independently established
H_2S [15]	≈+500 Hz at 10 ppb H_2S n.v. Definition: not established from the available source information	n.v.	10 ppb (reported test point; full range unresolved)	n.v. NR/not independently established
H_2S [42]	Frequency shift: −11.57 kHz at 10 ppm; −2.8 kHz at 0.5 ppm under 590 nm illumination 1.08306 kHz/ppm Definition: Linear fit of |Δf| over 0.5–8 ppm; $R^2 = 0.981$	0.5–50 ppm H_2S	0.5 ppm = 500 ppb	95.2 ppb in calculation; 31.8 ppb in conclusion (unresolved) LOD-U: numerical inconsistency
H_2S [18]	n.v. n.v. Definition: not established from the available source information	5 ppb–100 ppm H_2S	5 ppb	n.v. NR/not independently established

Table A2. *Cont.*

Gas [Ref.]	Readout/Reported Sensitivity/ Calibration Definition	Measured Interval	Minimum Tested	Author LOD/ Evidence Class
CO [43]	1.1 kHz at 10 ppm; 13.6 kHz at 100 ppm n.v. (endpoint secant only; no global fitted slope) Definition: Raw responses at endpoints only	10–100 ppm	10 ppm	n.v. MTC (measured concentration, not statistical LOD)
CO_2 [13]	~43 mV at 4 vol% CO_2 11.35 mV/vol% Definition: not established from the available source information	0.1–4 vol% CO_2	0.1 vol%	n.v. MTC (measured concentration, not statistical LOD)
CO_2 [44]	n.v. ~0.003 kHz/ppm (3 Hz/ppm) Definition: Published linear calibration slope	500–2000 ppm CO_2	500 ppm	n.v. LOD-U (procedure unresolved)
VOC (acetone/ethanol/to [14]	Negative Δf, calibrations; 5 ppm exposure for kinetics 910/742/340 Hz/ppm for acetone/ethanol/toluene Definition: Frequency shift/concentration change; Figure 5 of ref [14]	0.5–5 ppm acetone, ethanol, toluene	0.5 ppm = 500 ppb acetone	3/5/20 ppb est for acetone/ethanol/toluene LOD-U (SNR ≥ 3 criterion; statistic/calculation incomplete)
DMMP/DPGME [17]	Not verified 3087 Hz/ppm DMMP; 760 Hz/ppm DPGME Definition: Author-reported gas-specific sensitivities	DMMP down to 0.2 ppm; DPGME down to 0.75 ppm	DMMP 0.2 ppm; DPGME 0.75 ppm	9 ppb DMMP; 40 ppb DPGME LOD-U (procedure unresolved)
HCl [45]	~−1.4 kHz at 0.05 ppm n.v. Definition: Single response point, not global sensitivity	0.05 ppm point	≤0.05 ppm (confirmed test)	No statistical LOD in publisher abstract MTC (measured concentration, not statistical LOD)

n.v. = not verified in the examined source. The alternating row shading is used only to improve readability. The arrow (→) indicates the change from the untreated to the treated sensing layer. Both frequency shifts were measured at 10 ppm NO_2.

Table A3. Response dynamics, analytical limitations and verification scope for the same 32 records. Reported response/recovery values retain the source definition; absence of a verified value is not evidence of no response.

Gas [Ref.]	Response/Recovery	Analytical Qualification	Source Verification Scope
H_2 [12]	12–16 s (T90 at studied H_2 concentrations)	The reported 59 ppm LOD was estimated from sensitivity and baseline noise. The lowest H_2 exposure was 2000 ppm.	Original methods and Table 1 of reference [12].
H_2 [20]	Approximately 24/30 s at 0.4 vol% H_2 for Pd-700/SnO_2-700; source Figure 9 of ref [20]	3 × 10/0.21 ≈ 143 ppm matches reported 142 ppm within rounding; noise statistic remains unspecified; minimum test 2000 ppm.	Full-text methods and results examined; no independent raw-data reanalysis.
H_2 [22]	~7 s; half-year variation 3.7%	Est. LOD < 10 ppm vs. 100 ppm minimum actual measurement; 3× max noise/S diagnostic not statistical proof.	Full-text methods and results examined; no independent raw-data reanalysis.
H_2 [11]	<2 s/<4 s reported	Voltage readout cannot be compared directly with Hz/ppm; independent replication across related publications is not established.	Published values retained; full methodological verification is limited.
H_2 [21]	15–45 s response across gas exposures	Nominal 3 × 40/0.10 = 1200 ppm vs. tabulated 1210 ppm; rounding is consistent with this small difference. LOD < min tested 2000 ppm.	Full-text methods and results examined; no independent raw-data reanalysis.
CH_4 (also H_2) [8]	n.v.	At 200 ppm, 3 × 25/18 ≈ 4.17 ppm; author values retained; no challenge at 4.17 ppm.	Full-text methods and results examined; no independent raw-data reanalysis.
CH_4 [9]	n.v.	3 × 10/1.79 ≈ 16.8 ppm agrees with reported 17 ppm within rounding; minimum test 4000 ppm; noise statistic unverified.	Full-text methods and results examined; no independent raw-data reanalysis.

Table A3. *Cont.*

Gas [Ref.]	Response/Recovery	Analytical Qualification	Source Verification Scope
CH_4 [26]	16.7/66.4 s at 500 ppm; 36.4/31.2 s at 20 ppm	Section 4.1 reports 0.19 mV/ppm (1–20 ppm); conclusion 0.06 mV/ppm; abstract 0.046 mV/ppm (100–1000 ppm). Preserve native voltage readout and separate calibration windows; low-range conflict not resolvable from reported fit alone.	Full-text methods and results examined; no independent raw-data reanalysis.
CH_4 [25]	~12/~20 s at 5 vol%	Humidity modifies response; LOD estimated below 2000 ppm lowest tested; the quoted response/recovery times apply to the 5 vol% exposure.	Full-text methods and results examined; no independent raw-data reanalysis.
NH_3 [27]	30/60 s at 500 ppb NH_3; concentration-dependent response/recovery; source Table 1 of ref [27]	Estimated 425 ppb vs. 500 ppb minimum tested; 31-day response retention 54%; $R^2 = 0.9238$.	Full-text methods and results examined; no independent raw-data reanalysis.
NH_3 [28]	Response 200–1800 s; recovery 230–2400 s (0.5–50 ppm)	500 ppb is minimum experimental concentration, not validated 3σ LOD; strong concentration dependence of kinetics.	Full-text methods and results examined; no independent raw-data reanalysis.
NH_3 [32]	130/96 s at 12 ppb NH_3; source Table 2 of ref [32]	At 12 ppb Δf = 352 Hz and stated noise = 75 Hz: SNR = 4.69; 3 × 12/4.69 ≈ 7.7 ppb. This differs from 3 × 75/(2 Hz/ppb) = 112.5 ppb using the global reported slope. The noise statistic is not independently calibrated; neither estimate is an experimentally demonstrated concentration threshold. Aging/RH affect response.	Full-text methods and results examined; no independent raw-data reanalysis.
NH_3 [31]	n.v.	4878 Hz/ppm matches the 5 ppm point ratio, not a fitted slope over 5–50 ppm; <1 ppm claimed without reproducible derivation; minimum test 5 ppm.	Full-text methods and results examined; no independent raw-data reanalysis.
NH_3 [29]	n.v.	Source Figure 6 of ref [29] (80% RH) and the calibration in Figure 8 of ref [29] (50% RH) use different protocols; the 1 ppm limit is a tested point.	Full-text methods and results examined; no independent raw-data reanalysis.
NH_3 [30]	At 100 ppm: NRs 151/568 s; at 10 ppm NRs 266/431 s	ZnO NRs increase S approximately 3.8-fold but recovery 568 s at 100 ppm; 60-day stability reported; a quantitative drift metric was not extracted.	Full-text methods and results examined; no independent raw-data reanalysis.
NH_3 [19]	5/25 s	Single 100 ppm point ≠ sensitivity slope; humidity reverses sign; LOD derivation not established from the available source information.	Publisher or author–institution summary; full methods and raw baseline unavailable for verification.
NO_2 [34]	42/22 s	The 27 °C results are distinguished from elevated-temperature tests up to 200 °C.	Published values retained; full methodological verification is limited.
NO_2 [35]	131/116 s	Title says sub-ppb but abstract numerical LOD ~42 ppb; classify UV-assisted.	Published values retained; full methodological verification is limited.
NO_2 [16]	487/302 s untreated vs. 45/58 s treated	Sign reversal; cannot assign mechanism from signal sign alone.	Published values retained; full methodological verification is limited.
NO_2 [36]	n.v.	Source identifies σ as standard error of slope (degrees/ppm), so 3.3σ/S is dimensionless, not ppm; the stated ppb LODs lack a dimensionally reproducible derivation. Also 0.29 vs. 0.2°/ppm conflict; raw phase noise not available.	Full-text methods and results examined; no independent raw-data reanalysis.
NO_2 [37]	50.2/104 s	The 6.6 ppb estimate is distinct from the 20 ppb minimum tested concentration.	Publisher or author–institution summary; full methods and raw baseline unavailable for verification.

Table A3. *Cont.*

Gas [Ref.]	Response/Recovery	Analytical Qualification	Source Verification Scope
NO [39]	59/17 s at 80 ppb NO	Dry-air carrier; related to the earlier N_2 study [38], whose data are also discussed in the later publication.	Published values retained; full methodological verification is limited.
NO [38]	97/37 s at 10 ppb	Dry N_2 carrier; distinct gas matrix from the related dry-air study [39]. Previously reported N_2 results are not counted as independent replication in the later paper.	Full-text methods and results examined; no independent raw-data reanalysis.
H_2S [15]	n.v.	Mechanism attribution not proven from positive sign alone.	Publisher or author–institution summary; full methods and raw baseline unavailable for verification.
H_2S [42]	27/21 s at 10 ppm H_2S under 590 nm light; Figure 7c of ref [42]	SD = 0.0344 kHz from 300 baseline points; S = 1.08306 kHz/ppm over 0.5–8 ppm. Thus 3SD/S ≈ 95.3 ppb, whereas SD/S ≈ 31.8 ppb. Both published LOD values are retained; minimum tested: 500 ppb.	Full-text methods and results examined; no independent raw-data reanalysis.
H_2S [18]	n.v.	The 5 ppb value is a minimum tested concentration; a statistical LOD was not established.	Published values retained; full methodological verification is limited.
CO [43]	33.4/37.2 s (90% criterion)	Endpoint secant ≠ calibrated S; nitrogen as reference, not automatically air.	Full-text methods and results examined; no independent raw-data reanalysis.
CO_2 [13]	9.3/28.9 s	0.1 vol% is the minimum tested CO_2 concentration.	Full-text methods and results examined; no independent raw-data reanalysis.
CO_2 [44]	9/9.2 s at 700 ppm	Optically assisted RT; distinguish humidity mass loading from CO_2 positive shift.	Published values retained; full methodological verification is limited.
VOC (acetone/ethanol/toluene [14]	Acetone < 2.5 min response/<4 min recovery	30% RH suppresses acetone signal approximately sevenfold vs. dry; after humidity exposure dry response falls ~35%. 3 ppb LOD vs. 500 ppb minimum actually tested.	Full-text methods and results examined; no independent raw-data reanalysis.
DMMP/DPGME [17]	Not verified	Separate analyte-specific calibrations in one publication. LOD 9 ppb vs. minimum tested 200 ppb for DMMP; 40 ppb vs. minimum tested 750 ppb for DPGME.	Published values retained; full methodological verification is limited.
HCl [45]	n.v.	The 300 °C temperature refers to film annealing; sensing was performed at 25 °C.	Published values retained; full methodological verification is limited.

n.v. = not verified in the examined source. The alternating row shading is used only to improve readability.

Table A4 provides the numerical inputs for Figure 3. The ratio is G = Cmin,tested/LODreported, with both concentrations expressed on the same gas-fraction basis (1 vol% = 10,000 ppm; 1 ppm = 1000 ppb). It describes the separation between the minimum tested concentration and an author-reported LOD; it does not validate that LOD or rank sensors across gases. Both conflicting Bi_2S_3 LOD reports are retained.

Table A4. Input concentrations and ratios underlying Figure 3. Ratios are displayed to two decimal places; the graph uses the unrounded ratios.

Gas/Film [Ref.]	Minimum Tested	Author LOD	G	Qualification
H_2/Pd–ZnO [12]	2000 ppm	59 ppm	33.90	Descriptive ratio only; author LOD retained
H_2/Pd–SnO_2 [20]	2000 ppm	142 ppm	14.08	Descriptive ratio only; author LOD retained
H_2/Pd–Ni nanowires [11]	3000 ppm	7 ppm	428.57	Descriptive ratio only; author LOD retained
H_2/Pd–TiO_2 [21]	2000 ppm	1210 ppm	1.65	Descriptive ratio only; author LOD retained

Table A4. *Cont.*

Gas/Film [Ref.]	Minimum Tested	Author LOD	G	Qualification
CH_4/plasma-treated CNWs [8]	200 ppm	4.17 ppm	47.96	Descriptive ratio only; author LOD retained
CH_4/W,V:TiO_2–Pd–PEI [9]	4000 ppm	17 ppm	235.29	Descriptive ratio only; author LOD retained
NH_3/rGO–DPP2T-TT [27]	500 ppb	425 ppb	1.18	Descriptive ratio only; author LOD retained
NH_3/AuNPs–Cu_2O/rGO/PPy [32]	12 ppb	8 ppb	1.50	Descriptive ratio only; author LOD retained
NO_2/Pt nanoclusters–GO [37]	20 ppb	6.6 ppb	3.03	Descriptive ratio only; author LOD retained
H_2S/Bi_2S_3, yellow light [42]	500 ppb	95.2 ppb Alternative: 31.8 ppb	5.25 Alt.: 15.72	Both limits disputed

The alternating row shading is used only to improve readability.

Table A5. Source-traceable numerical and methodological limitations relevant to interpreting Tables 3, 4 and A1–A4. These diagnostic calculations are not substitutes for publication-author corrections or validation from raw data.

Case [Ref.]	Published Quantity/Boundary	Independent Diagnostic or Caveat	Decision for Review
H_2 Pd–Ni [22]	<10 ppm in results; 10 ppm conclusion; 100 ppm minimum	Source's noise is not a documented blank standard deviation.	Retain two source wordings; lowest measured = 100 ppm.
CH_4 carbon nanowalls [8]	4.17 ppm author LOD; 200 ppm minimum	3 × 25 Hz/(18 Hz/ppm) = 4.17 ppm at the cited point; one-point coefficient.	Single-point extrapolation, not direct 4.17 ppm exposure.
CH_4 W,V:TiO_2/Pd–PEI [9]	17 ppm author LOD; 4000 ppm minimum	3 × 10 Hz/(1.79 Hz/ppm) = 16.8 ppm; exact blank-noise estimator unavailable.	Report LOD-U and very large validation gap.
NH_3 AuNPs–Cu_2O/rGO/PPy [32]	8 ppb author LOD; 12 ppb minimum	3 × 12 ppb/(352/75) = 7.7 ppb; using global 2 Hz/ppb yields 112.5 ppb as diagnostic.	LOD-R; distinguish point SNR from global slope.
NH_3 MoS_2 [31]	4878 Hz/ppm at 5 ppm; 5–50 ppm investigated	24,389/5 = 4877.8 Hz/ppm; [107,668 − 24,389]/45 ≈ 1850.6 Hz/ppm.	Point ratio ≠ fitted full-domain sensitivity.
NO_2 UV/g-C_3N_4 [35]	"sub-ppb" title; ≈42 ppb in abstract	1 ppb is smaller than 42 ppb; both wordings appear in one source.	Use numeric ≈ 42 ppb, UV-assisted, author estimate.
NO_2 graphene phase [36]	68/140 ppb author LODs; slope SE used as σ	The slope standard error and the fitted slope are both expressed in degrees/ppm. Therefore, 3.3σ/S is dimensionless.	LOD-U until output-noise/relevant statistic identified.
H_2S Bi_2S_3 [42]	95.2 ppb methods; 31.8 ppb conclusion; min 500 ppb	3 × 0.0344 kHz/(1.08306 kHz/ppm) ≈ 95.3 ppb; omitting the factor 3 gives ≈31.8 ppb.	Use formula-consistent ≈95.2 ppb descriptively; flag contradiction.
NO [38,39]	Related source papers in N_2 vs. air	The 2017 paper recaps earlier nitrogen testing; distinct DOI ≠ independent duplicate experiment.	Previously reported dry-N_2 results are not independent replication.
CO_2 SnO_2/CuO [13]	11.35 mV/vol%; 0.1–4 vol% tested	Voltage from phase-to-voltage circuitry.	Voltage sensitivity is not directly comparable with Hz/ppm.

The alternating row shading is used only to improve readability.

All reported thresholds below the minimum tested concentration are extrapolations. "Unresolved" means that independent verification was not possible from the accessible original reports; it does not imply that the reported sensor response is false.

References

1. Dinu, L.A.; Buiculescu, V.; Baracu, A.M. Recent Progress on Nanomaterials for NO_2 Surface Acoustic Wave Sensors. *Nanomaterials* **2022**, *12*, 2120. [CrossRef] [PubMed]
2. Li, X.; Sun, W.; Fu, W.; Lv, H.; Zu, X.; Guo, Y.; Gibson, D.; Fu, Y.Q. Advances in sensing mechanisms and micro/nanostructured sensing layers for surface acoustic wave-based gas sensors. *J. Mater. Chem. A* **2023**, *11*, 9216–9238. [CrossRef]
3. Lin, Q.; Zhao, C.; Li, M.; Xu, H. Recent Progress in Surface Acoustic Wave Sensors Based on Low-Dimensional Materials and Their Applications. *Chemosensors* **2024**, *12*, 255. [CrossRef]
4. Reddeppa, M.; Thota, C.; Choppara, S.; Murali, G.; Kumar, A.; Kim, M.D. A review on 2D materials for surface acoustic wave gas sensors at room temperature. *J. Mater. Chem. A* **2025**, *13*, 11921–11951. [CrossRef]
5. Wohltjen, H.; Dessy, R. Surface acoustic wave probe for chemical analysis. I. Introduction and instrument description. *Anal. Chem.* **1979**, *51*, 1458–1464. [CrossRef]
6. Wohltjen, H. Mechanism of operation and design considerations for surface acoustic wave device vapour sensors. *Sens. Actuators* **1984**, *5*, 307–325. [CrossRef]
7. Ricco, A.J.; Martin, S.J.; Zipperian, T.E. Surface acoustic wave gas sensor based on film conductivity changes. *Sens. Actuators* **1985**, *8*, 319–333. [CrossRef]
8. Vizireanu, S.; Constantinoiu, I.; Satulu, V.; Stoica, S.D.; Viespe, C. High-Sensitivity H_2 and CH_4 SAW Sensors with Carbon Nanowalls and Improvement in Their Performance after Plasma Treatment. *Chemosensors* **2023**, *11*, 566. [CrossRef]
9. Scarisoreanu, M.; Constantinoiu, I.; Goncearenco, E.; Morjan, I.P.; Teodorescu, V.S.; Viespe, C. The Effect of Loading W&V:TiO_2 Nanoparticles with Noble Metals for CH4 Detection. *Chemosensors* **2024**, *12*, 160. [CrossRef]
10. Liu, X.; Wang, W.; Zhang, Y.; Pan, Y.; Liang, Y.; Li, J. Enhanced Sensitivity of a Hydrogen Sulfide Sensor Based on Surface Acoustic Waves at Room Temperature. *Sensors* **2018**, *18*, 3796. [CrossRef] [PubMed]
11. Wang, X.; Du, L.; Cheng, L.; Zhai, S.; Zhang, C.; Wang, W.; Liang, Y.; Yang, D.; Chen, Q.; Lei, G. Pd/Ni nanowire film coated SAW hydrogen sensor with fast response. *Sens. Actuators B Chem.* **2022**, *351*, 130952. [CrossRef]
12. Viespe, C.; Miu, D. Surface Acoustic Wave Sensor with Pd/ZnO Bilayer Structure for Room Temperature Hydrogen Detection. *Sensors* **2017**, *17*, 1529. [CrossRef] [PubMed]
13. Jin, J.; Yang, Q.; Hu, A.; Cui, B.; Xue, X.; Liang, Y.; Shi, F.; Lee, K.; Wang, W. Heterojunction interface-engineered SnO_2-CuO SAW sensor for room-temperature CO_2 detection with fast response and high selectivity. *Microsyst. Nanoeng.* **2025**, *11*, 226. Correction in *Microsyst. Nanoeng.* **2026**, *12*, 75. https://doi.org/10.1038/s41378-026-01223-2. [CrossRef] [PubMed]
14. Šetka, M.; Bahos, F.A.; Matatagui, D.; Gràcia, I.; Figueras, E.; Drbohlavová, J.; Vallejos, S. Love Wave Sensors with Silver Modified Polypyrrole Nanoparticles for VOCs Monitoring. *Sensors* **2020**, *20*, 1432. [CrossRef] [PubMed]
15. Tang, Y.; Xu, X.; Han, S.; Cai, C.; Du, H.; Zhu, H.; Zu, X.; Fu, Y. ZnO-Al_2O_3 nanocomposite as a sensitive layer for high performance surface acoustic wave H2S gas sensor with enhanced elastic loading effect. *Sens. Actuators B Chem.* **2020**, *304*, 127395. [CrossRef]
16. Li, M.; Kan, H.; Chen, S.; Feng, X.; Li, H.; Li, C.; Fu, C.; Quan, A.; Sun, H.; Luo, J.; et al. Colloidal quantum dot-based surface acoustic wave sensors for NO_2-sensing behavior. *Sens. Actuators B Chem.* **2019**, *287*, 241–249. [CrossRef]
17. Sayago, I.; Matatagui, D.; Fernández, M.J.; Fontecha, J.L.; Jurewicz, I.; Garriga, R.; Muñoz, E. Graphene oxide as sensitive layer in Love-wave surface acoustic wave sensors for the detection of chemical warfare agent simulants. *Talanta* **2016**, *148*, 393–400. [CrossRef] [PubMed]
18. Tang, Y.; Wu, W.; Wang, B.; Dai, X.; Xie, W.; Yang, Y.; Zhang, R.; Shi, X.; Zhu, H.; Luo, J.; et al. H_2S gas sensing performance and mechanisms using CuO-Al_2O_3 composite films based on both surface acoustic wave and chemiresistor techniques. *Sens. Actuators B Chem.* **2020**, *325*, 128742. [CrossRef]
19. Bak, N.H.; Pasupuleti, K.S.; Maddaka, R.; Shim, Y.H.; Pham, T.T.M.; Kim, Y.H.; Kim, M.D. Ultrafast Detection of ppb-Level NH_3 Gas at Room Temperature Using CuO Nanoparticles Decorated AlN-Based Surface Acoustic Wave Sensor. *ACS Sens.* **2025**, *10*, 709–716. [CrossRef] [PubMed]
20. Constantinoiu, I.; Miu, D.; Viespe, C. SAW Hydrogen Sensors with Pd/SnO_2 Layers. *Materials* **2022**, *15*, 8012. [CrossRef] [PubMed]
21. Constantinoiu, I.; Viespe, C. Development of Pd/TiO_2 Porous Layers by Pulsed Laser Deposition for Surface Acoustic Wave H_2 Gas Sensor. *Nanomaterials* **2020**, *10*, 760. [CrossRef] [PubMed]
22. Wang, W.; Liu, X.; Mei, S.; Liu, M.; Lu, C.; Lu, M. Development of a High Stability Pd-Ni Alloy Thin-Film Coated SAW Device for Sensing Hydrogen. *Sensors* **2019**, *19*, 3560. [CrossRef] [PubMed]
23. Wang, W.; Liu, X.; Mei, S.; Jia, Y.; Liu, M.; Xue, X.; Yang, D. Development of a Pd/Cu nanowires coated SAW hydrogen gas sensor with fast response and recovery. *Sens. Actuators B Chem.* **2019**, *287*, 157–164. [CrossRef]
24. Constantinoiu, I.; Viespe, C. Hydrogen Detection with SAW Polymer/Quantum Dots Sensitive Films. *Sensors* **2019**, *19*, 4481. [CrossRef] [PubMed]
25. Wang, W.; Hu, H.; Liu, X.; He, S.; Pan, Y.; Zhang, C.; Dong, C. Development of a Room Temperature SAW Methane Gas Sensor Incorporating a Supramolecular Cryptophane A Coating. *Sensors* **2016**, *16*, 73. [CrossRef] [PubMed]

26. Guo, D.; Jin, J.; Yang, Q.; Sun, L.; Jia, J.; Wang, W. Detection of Methane at ppm Level Using Monolayer Graphene Oxide Film on Surface Acoustic Wave Device. *Appl. Sci.* **2026**, *16*, 7001. [CrossRef]
27. Hung, T.T.; Chung, M.H.; Wu, J.Y.; Shen, C.Y. A Room-Temperature Surface Acoustic Wave Ammonia Sensor Based on rGO/DPP2T-TT Composite Films. *Sensors* **2022**, *22*, 5280. [CrossRef] [PubMed]
28. Wang, W.; Guo, Y.; Xiong, W.; Fu, Y.; Elmarakbi, A.; Zu, X. Highly Sensitive and Selective Surface Acoustic Wave Ammonia Sensor Operated at Room Temperature with a Polyacrylic Acid Sensing Layer. *Sensors* **2022**, *22*, 6349. [CrossRef] [PubMed]
29. Zhao, L.; Wang, R.; Cao, Q. Highly Sensitive Surface Acoustic Wave NH_3 Gas Sensor based on TiO_2 Film. *Sens. Mater.* **2020**, *32*, 4111–4119. [CrossRef]
30. Li, W.; Guo, Y.; Tang, Y.; Zu, X.; Ma, J.; Wang, L.; Fu, Y.Q. Room-Temperature Ammonia Sensor Based on ZnO Nanorods Deposited on ST-Cut Quartz Surface Acoustic Wave Devices. *Sensors* **2017**, *17*, 1142. [CrossRef] [PubMed]
31. Chung, C.Y.; Chen, Y.C.; Juang, F.R.; Kao, K.S.; Lee, E.I. Preparation of MoS_2 Nanospheres using a Hydrothermal Method and Their Application as Ammonia Gas Sensors Based on Delay Line Surface Acoustic Wave Devices. *Materials* **2023**, *16*, 4703. [CrossRef] [PubMed]
32. Pan, C.L.; Hung, T.T.; Shen, C.Y.; Chen, P.H.; Tai, C.M. Highly Sensitive Surface Acoustic Wave Sensors for Ammonia Gas Detection at Room Temperature Using Gold Nanoparticles–Cuprous Oxide/Reduced Graphene Oxide/Polypyrrole Hybrid Nanocomposite Film. *Polymers* **2025**, *17*, 1024. [CrossRef] [PubMed]
33. Shen, C.Y.; Hung, T.T.; Chuang, Y.W.; Lai, S.K.; Tai, C.M. Room-Temperature NH_3 Gas Surface Acoustic Wave (SAW) Sensors Based on Graphene/PPy Composite Films Decorated by Au Nanoparticles with ppb Detection Ability. *Polymers* **2023**, *15*, 4353. [CrossRef] [PubMed]
34. Pasupuleti, K.S.; Nam, D.J.; Bak, N.H.; Reddeppa, M.; Oh, J.E.; Kim, S.G.; Cho, H.D.; Kim, M.D. Highly sensitive g-C_3N_4 nanosheets as a potential candidate for the effective detection of NO_2 gas via langasite-based surface acoustic wave gas sensor. *J. Mater. Chem. C* **2022**, *10*, 160–170. [CrossRef]
35. Pasupuleti, K.S.; Vidyasagar, D.; Ambadi, L.N.; Bak, N.H.; Kim, S.G.; Kim, M.D. UV light activated g-C_3N_4 nanoribbons coated surface acoustic wave sensor for high performance sub-ppb level NO_2 detection at room temperature. *Sens. Actuators B Chem.* **2023**, *394*, 134471. [CrossRef]
36. Buiculescu, V.; Dinu, L.A.; Veca, L.M.; Pârvulescu, C.; Mihai, M.; Brîncoveanu, O.; Comănescu, F.; Brașoveanu, C.; Stoian, M.; Baracu, A.M. The development of sensitive graphene-based surface acoustic wave sensors for NO_2 detection at room temperature. *Microchim. Acta* **2024**, *191*, 323. [CrossRef] [PubMed]
37. Yang, Q.; Jin, J.; Hu, A.; Cui, B.; Xue, X.; Liang, Y.; Wang, W. Synergistic enhancement of room-temperature NO_2 sensing by Pt nanoclusters and SAW device. *Nano Res.* **2026**, *19*, 94908693. [CrossRef]
38. Wang, S.H.; Shen, C.Y.; Su, J.M.; Chang, S.W. A Room Temperature Nitric Oxide Gas Sensor Based on a Copper-Ion-Doped Polyaniline/Tungsten Oxide Nanocomposite. *Sensors* **2015**, *15*, 7084–7095. [CrossRef] [PubMed]
39. Wang, S.H.; Shen, C.Y.; Lien, Z.J.; Wang, J.H. Nitric oxide sensing properties of a surface acoustic wave sensor with copper-ion-doped polyaniline/tungsten oxide nanocomposite film. *Sens. Actuators B Chem.* **2017**, *243*, 1075–1082. [CrossRef]
40. Li, D.; Zu, X.; Ao, D.; Tang, Q.; Fu, Y.; Guo, Y.; Bilawal, K.; Faheem, M.B.; Li, L.; Li, S.; et al. High humidity enhanced surface acoustic wave (SAW) H_2S sensors based on sol–gel CuO films. *Sens. Actuators B Chem.* **2019**, *294*, 55–61. [CrossRef]
41. Lu, Y.; Wang, D.; Lv, W.; Xia, Y.; Ou, K.; Li, Y.; Du, Z.; He, Y.; Dai, J.; Wu, S.; et al. Surface acoustic wave hydrogen sulfide gas sensors based on porous SnO_2-SiO_2 composite films. *Sens. Actuators B Chem.* **2024**, *417*, 136117. [CrossRef]
42. Li, C.; Ramadan, S.; Kan, H.; Wang, L. Light-Activated Room Temperature Surface Acoustic Wave H_2S Sensor Based on Bi_2S_3 Nanoribbons. *Sensors* **2025**, *25*, 1122. [CrossRef] [PubMed]
43. Yang, H.; Shen, B.; Liu, X.; Jin, C.; Zhou, T. A Study on the Gas/Humidity Sensitivity of the High-Frequency SAW CO Gas Sensor Based on Noble-Metal-Modified Metal Oxide Film. *Sensors* **2023**, *23*, 2487. [CrossRef] [PubMed]
44. Wang, C.; Ding, Y.; Li, M.; Li, H.; Xu, S.; Li, C.; Qian, L.; Yang, B. Surface acoustic wave sensor based on Au/TiO_2/PEDOT with dual response to carbon dioxide and humidity. *Anal. Chim. Acta* **2022**, *1190*, 339264. [CrossRef] [PubMed]
45. Tang, Y.; Li, D.; Ao, D.; Guo, Y.; Faheem, M.B.; Khan, B.; Zu, X.; Li, S. Highly sensitive surface acoustic wave HCl gas sensors based on hydroxyl-rich sol-gel AlOxOHy films. *Mater. Chem. Phys.* **2020**, *239*, 122026. [CrossRef]
46. Shu, L.; Jiang, T.; Xia, Y.; Wang, X.; Yan, D.; Wu, W. The Investigation of a SAW Oxygen Gas Sensor Operated at Room Temperature, Based on Nanostructured ZnxFeyO Films. *Sensors* **2019**, *19*, 3025. [CrossRef] [PubMed]
47. Miu, D.; Birjega, R.; Viespe, C. Surface Acoustic Wave Hydrogen Sensors Based on Nanostructured Pd/WO_3 Bilayers. *Sensors* **2018**, *18*, 3636. [CrossRef] [PubMed]

Disclaimer/Publisher's Note: The statements, opinions and data contained in all publications are solely those of the individual author(s) and contributor(s) and not of MDPI and/or the editor(s). MDPI and/or the editor(s) disclaim responsibility for any injury to people or property resulting from any ideas, methods, instructions or products referred to in the content.